UNIVERSITY OF CALIFORNIA
RIVERSIDE

Comprehending Slow Earthquakes With a Multitude of Techniques

A Dissertation submitted in partial satisfaction
of the requirements for the degree of

Doctor of Philosophy
in
Earth and Planetary Sciences

by
Kuntal Chaudhuri

March 2022

Dissertation Committee:
Dr. Abhijit Ghosh, Chairperson
Dr. David D. Oglesby
Dr. Roby Douilly

This Dissertation of Kuntal Chaudhuri is approved

_____

_____

_____

Committee Chairperson

University of California, Riverside

ACKNOWLEDGMENT

This thesis is dedicated to my mom (Madhuchanda Chaudhuri), dad (Kisore Kumar Chaudhuri), and sister (Sayani Chaudhuri). Without your constant love, support, and encouragement, this would not have been possible. You are the best support system that I could have ever asked for.

I am grateful to Dr. Abhijit Ghosh. His ability to address and deconstruct arcane questions in geophysics is fantastic. His constant encouragement to tackle complex problems and prompt guidance has been the greatest motivation for my research.

Dr. David Oglesby has been an inspiring figure, and it has always been a pleasure talking to him. He has been one of the most supportive and helpful people I have come across. Thanks to Dr, Oglesby for giving me constant inspiration to keep working whenever I questioned myself.

I would also like to thank Gouri Chakraborty for her constant encouragement throughout my journey here. It would have been impossible without her help, care, and support.

I would also like to extend my gratitude to Dr. Gareth Funning and Dr. Roby Douilly. They are excellent scientists, and I have learned a lot from them in tackling various problems in all aspects of life.

I would like to thank the Department of Earth and Planetary Sciences of UCR for welcoming me here and making me a part of their family.

Finally, I would like to thank my college friends from IISER Kolkata and colleagues from the geophysics group of UCR. They have supported me immensely throughout my journey here.

As the saying goes, sharing is caring, so I would like to thank them all for always being there for me through my good and bad times and allowing me to be a part of their lives.

ABSTRACT OF THE DISSERTATION

Comprehending Slow Earthquakes With a Multitude of Techniques

by

Kuntal Chaudhuri

Doctor of Philosophy, Graduate Program in Earth and Planetary Sciences
University of California, Riverside, March 2022
Dr. Abhijit Ghosh, Chairperson

Tectonic stress is released in the form of aseismic and seismic signatures. Slow and fast/regular earthquakes represent different extremes the seismic spectrum and although we know a lot about the latter the mechanisms of slow earthquakes are still not very well understood. Ever since the discovery of slow earthquakes (Rogers & Dragert, 2003), seismic and geodetic observations and laboratory studies have helped elucidate the nature of these events whose nature varies a lot even amongst themselves. Slow earthquakes include low frequency earthquakes (LFEs), tremors, very low frequency earthquakes (VLFEs), slow slip events (SSE) and episodic tremor and slip (ETS Although their nature differs from location to location, they follow an empirical linear moment duration scaling law. Each of these events has a distinct signal duration and frequency range that makes its detection challenging. These events have often been observed to affect regular seismicity.

Studies have shown that slow earthquakes have often precede large regular earthquakes of different sizes and forms. A couple of slow earthquakes led up to the mainshock of the Mw 9.0 Tohoku earthquake 2011 (Kato et al., 2012). A foreshock

sequence associated with multiple slow-slip events spatiotemporally preceded the M_w 8.1 Iquique earthquake in 2014 (Kato & Nakagawa, 2014; Ruiz et al., 2014). Such evidence is not limited to only subduction zones. The M_w 7.9 Izmit earthquakes were also preceded by 44 minutes of slow earthquake activity characterized by long-period signals that increased until the mainshock (Bouchon et al., 2011). The most enigmatic example would be the transition of a VLFE into an Mw 3.7 earthquake in a strike-slip setting in Alaska (Tape et al., 2018). The fact that these transition slip behaviors can occur in the same part of the fault interface as regular earthquakes raise questions about the mechanism that transforms one type of slip behavior to another. The 2011 Tohoku earthquake ruptured a part of the fault previously associated with VLFE activity (Ide, Shelly, et al., 2007), raising questions about reassessing our understanding of basic fault mechanics.

The research shared herein analyses the physical processes behind spatiotemporal behavior of earthquakes, especially VLFEs, in various tectonic settings. The first project examines the offshore region of Cascadia subduction zone. The study begins in chapter 2 where we discover widespread occurrence of discrete VLFEs offshore Cascadia using ocean-bottom seismometers. Barring occasional regular fast earthquakes, VLFEs are the only seismic stress indicators in offshore CSZ. In the first section of Chapter 2, using centroid moment tensor inversion and matched filtering, we detected sequences of 12 distinct families of VLFEs. The VLFEs north of 43N have a focal mechanism consistent with subduction zone deformation in the area. However, the VLFEs, along 43N-46N, show strike-slip faulting, attributed to sediment consolidation, subduction bending, and transpressional regimes created by complex plate tectonics. It challenges a canonical view

of seismogenic zone in Cascadia characterized by a frictionally homogeneous fault segment producing only regular fast earthquakes. The second project involves the discovery of VLFEs and their temporal relationship to nearby regular earthquakes on the Island of Taiwan. This study detects discrete very low frequency earthquakes (VLFEs) using a grid search moment tensor inversion algorithm (Ghosh et al., 2015; Hutchison & Ghosh, 2019). By applying a matched filtered technique, we have created a robust VLFE catalog for three years. The two VLFEs closer to the tremor-producing region show a temporal relationship, but the western VLFE is the most active among the three. Our VLFE catalog of high temporal resolution allows us to identify a significant increase in VLFE activities preceding earthquake swarms. An empirical comparison of the VLFE catalog with regional and local cataloged fast earthquakes reveal two such instances. We show that fluid migration from deeper to shallower crust explains this modulation of regular fast earthquakes by VLFEs. In the following chapter we use Beam Back Projection (BBP) to detect and located tremors in Cholame. Our results show five times more detections than the conventional ECC method. The use of beam back-projection (BBP) has helped us to identify shallow tremors that have never been observed before in this area. We have strong evidence showing persistent shallow tremor activity in the seismogenic zone with our high-resolution seismic array. We create a robust catalog of events for one year and show that the presence of high fluid pressure may be attributed to the crustal heterogeneity that we observe. In the final chapter of this study, we use the experience from the two projects discussed above and create a robust automatic VLFE detection code package. This code can detect, locate, and provide a matched filtered catalog of all events occurring within a

user specified region. Earlier all these parts have been used separately and the method was more prone to systematic and human error. We use 2 datasets to verify our observations and finally make the code package publicly available for use. In summary, this research portrays how important slow earthquakes are in the grander scheme of plate tectonics which can improve our understanding of plate interactions.

Table of Contents

List of Figures

CHAPTER 1

1.1 Introduction

Seismic stress release varies in a wide range of the frequency spectrum. The earthquakes that we are most familiar with are the ones that shake the surroundings but only belong to just one end member of the slip behavior. We can also observe other fault behaviors with improved detection technology, better instrument coverage, and fast-evolving computational techniques. This newly observed fault behavior opens our understanding of plate response to tectonic stresses. Not only do they help us characterize fault behavior, but also to understand the mechanism behind complexities we see in fault slip. Another end of the spectrum belongs to aseismic creep, which cannot be observed with seismicity, but instead through strain alone. The last couple of decades has seen the emergence of an entire gray area of slip spectrum that includes both seismic and aseismic slip elements. A new set of tools has evolved to explore this phenomenon, and it will also help us understand and modify the previous theories. This dissertation explores various kinds of slow earthquake behavior to better understand their role in subduction zone mechanics.

1.2 The Slip Spectrum

Faults show a complex range of slip behavior mainly dependent on stress and frictional properties, which are dependent on the composition of the rock. Moreover, the behavior of the rocks is controlled by temperature, pressure, and water content, particularly clear in subduction zones. Fast earthquakes in the subduction zone rupture suddenly when their frictional stress to fault movement drops faster than the elastic stress due to fault slip,

followed by periods of no motions as stress reloads (Schwartz & Rokosky, 2007). However, the moment released by these large earthquakes is only a fraction of the total moment due to plate tectonic motions (Frank, 2016). Further below the seismogenic zone, the plates cannot reach such high velocities for regular earthquakes. This stress gets released in low amplitude and low-frequency seismic signals, known as slow earthquakes (Z. Peng & Gomberg, 2010). Tremors, LFEs and VLFEs constitute much of the slow earthquake spectrum. This study analyzes these events in Taiwan, Cascadia, and Parkfield, California.

1.3 Slow Earthquakes

Empirically slow earthquakes follow a different scaling relationship than regular fast earthquakes based on their moment rate or how much moment is produced per unit time. Regular earthquakes have their moment proportional to the cube of their duration. However, slow earthquakes instead follow a linear relationship, hence aptly named 'slow' (Ide, Beroza, et al., 2007; Ide, Shelly, et al., 2007). Slow earthquakes is a broad term encompassing all events that do not behave like an aseismic creep or regular earthquakes. Slow slipping events (SSE), are discrete aseismic slip events, can produce events with a magnitude as large as Mw 7. Very Low frequency earthquakes (VLFEs) produce the most significant seismic moment of slow seismic earthquakes with prominent energy in the 0.02 - 0.05 Hz. Their signal durations are around 90-110 secs and generally produce events with Mw 3-4. Low frequency earthquakes (LFEs) produce short-duration signals instead, usually lasting no more than 10 seconds, and are typically depleted of energy outside the 1-10 Hz band. These are short events, and tremors are often considered to be clustered

LFEs since these are difficult to isolate, making it challenging to quantify the moment release of tremor. These slow earthquakes have distinctive seismic signatures that distinguish them from regular earthquakes (Figure 1.1). Another spectrum of slow earthquakes, which is out of the scope of this dissertation, is ultra-low frequency earthquakes which have also been observed in the electromagnetic spectrum (Hayakawa et al., 2007).

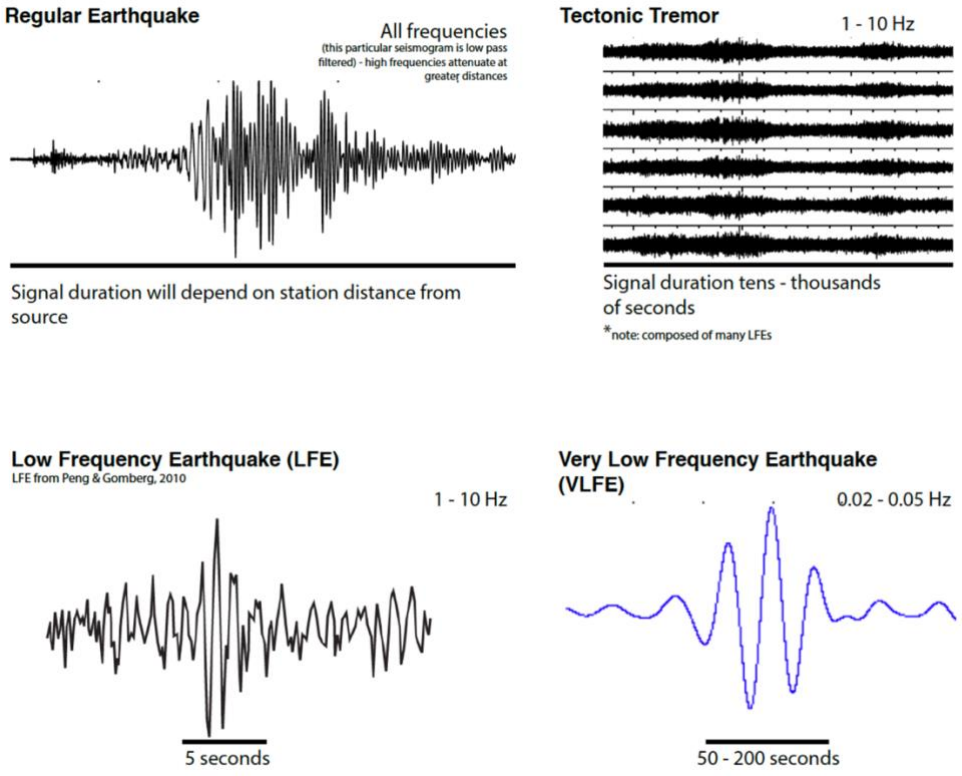

Figure 1.1: This figure gives examples of each of the main types of seismic slow earthquakes compared to a regular earthquake. The upper left-hand corner demonstrates a regular earthquake in the upper left-hand corner. They emit energy at all frequency bands, but higher frequencies attenuate at greater distances. There are distinct and impulsive P- and S- wave arrivals. A low frequency earthquake (LFE) is shown in the lower left-hand corner (Z. Peng & Gomberg, 2010). They emit energy between 1-10 Hz and have short signal durations (5-10s). In the upper right-hand corner is an example of tremor. Tremor consists of the clustered arrivals of many LFEs and thus has the same frequency content. Tremor, like the other events, must be coherent across multiple stations, preferably network stations. It can last from tens to thousands of seconds. Finally, an example of a very low frequency earthquake (VLFE) is shown in the lower right-hand corner. It is completely depleted of high frequency energy and primarily emits energy in the 0.02 - 0.05 Hz frequency band. The signal duration is typically from 50 - 200 seconds.

1.4 Tremors

Until the discovery of slow earthquakes in 2002-2003 (Obara, 2002; Rogers & Dragert, 2003), the slip was considered bimodal to produce seismic energy (aseismic slip or regular fast earthquakes). Many models were constructed, and experiments were conducted to fit the bi-modal slip behavior theory better. Different physical and chemical properties can determine how and when a fault can slip, and these are often dependent on depth and the geologic setting. The plasticity of the crustal rocks increases with increasing temperature and depth, and materials tend to deform less brittle, which means that slip occurs with little to no frictional resistance or elastic deformation. Shallower crust often shows similar behavior, primarily attributed to fluid percolation decreasing normal stresses. Tremors are one manifestation of such a stress release in transition zones. Tectonic tremors (TTs), also known as Non-volcanic tremors (NVTs), are characterized by non-harmonic emergent signals of sustained amplitude lasting from minutes to days and sometimes even months. They were first observed in the Nankai trough subduction zone in Southwest Japan by Obara, 2002 An apparent distinguishing factor other than its non-emergent nature is its dominant frequency range. Compared to fast earthquakes, their peak energy lies between 1-10 Hz and is depleted in higher frequencies like regular earthquakes. In many other areas, including Cascadia (Rogers & Dragert, 2003), Mexico (Payero et al., 2008), Costa Rica (Brown et al., 2009; Feng et al., 2012), and Alaska (Peterson et al., 2011), tremors were also discovered. Recently, TTs were observed under San Andreas Fault, a transform plate boundary (Nadeau & Dolenc, 2005), and beneath the central range in Taiwan, an arc continental type collision environment (Chao et al., 2012). These TTs

have been seen to migrate along the transition zone of the plate interface. Observations in Japan strongly suggest that tremor outlines the depth of slip in megathrust earthquakes (Ide, Shelly, et al., 2007). Thus, the study of tremors provides us with an opportunity to study the poorly understood region largely devoid of seismicity (Rubinstein et al., 2009).

Slip events accompanied by tremors were first observed in Cascadia and Southwest Japan (Hirose et al., 1999; Rogers & Dragert, 2003). SSEs release accumulated plate boundary strain with duration in the order of days to years, without radiating detectable seismic energy, hence cannot be detected using conventional seismic arrays used for regular earthquake monitoring. SSEs have been detected in multiple subduction zones using Global Positioning System (GPS) networks, and their duration varies to a wide range (Dragert et al., 2001; Kostoglodov et al., 2010; Ozawa et al., 2001; Schwartz & Rokosky, 2007; Yamamoto et al., 2005). The discovery of SSEs has improved our understanding of the total moment release in varus tectonic settings since regular earthquakes constitute only a fraction of the strain accumulation and stress release (Frank, 2016). Since SSEs mainly occur in the transition zone, they can sometimes increase the stress in the shallower crust, seating regular earthquakes (Kato et al., 2012). The coupled phenomenon among tremors and SSEs gives us a new approach to study slow slip events wherever GPS data are limited and help to assess better seismic hazard (Schwartz & Rokosky, 2007). Rivet et al., 2011, recently observed a change in the seismic velocity changes near the subduction interface of the Mexican subduction zone during periods of intense TT activity temporally coherent with other SSEs. Tremor migration is an important feature that provides clues about the dynamics of slow earthquakes (Ghosh, Vidale, Sweet, Creager, Wech, & Houston, 2010;

Ghosh, Vidale, Sweet, Creager, Wech, Houston, et al., 2010). This TT activity can be used to track transient strain at depth and help us know more about the conditions of some deep-rooted fault zones and hence help in the possibility of greater predictability of larger earthquakes.

1.5 Low Frequency and Very Low-Frequency Earthquakes

Since 1999, the Japan Meteorological Agency (JMA) has differentiated a class of different events from regular fast earthquakes, denoted as low-frequency earthquakes (LFEs), in their seismicity catalog. LFEs are small earthquakes (less than Mw 2) with amplitudes that fall off much faster than regular earthquakes at higher frequencies (greater than 10 Hz) (Katsumata & Kamaya, 2003; Shelly et al., 2006). Earlier studies showed that LFE comprises at least a portion of the tremor (Shelly et al., 2007a, 2007b), and the spectral characteristics are nearly identical. LFEs and TT occur in approximately the same region and exhibit similar migration along the fault strike. Brown et al., 2009 showed that LFEs comprise tremors on the plate interface downdip of the locked portion of the subduction zone. This close association implies that their mechanisms might be intertwined. Thus, locating these slow earthquakes are imperative in understanding tremors as a whole. Shelly et al., 2006 shows a strong indication that the LFEs occur on the plate interface, coinciding with the inferred zone of slow slip. Thus, LFEs could also present another way to observe slow-slip at depth, possibly contributing to seismic hazard forecasting.

Many Recent studies show growing evidence of slow earthquakes preceding regular earthquakes in different sizes and forms. A couple of slow earthquakes led up to the mainshock of the Mw 9.0 Tohoku earthquake 2011 (Kato et al., 2012). A foreshock

sequence associated with multiple slow-slip events spatiotemporally preceded the M_w 8.1 Iquique earthquake in 2014 (Kato & Nakagawa, 2014; Ruiz et al., 2014). Such evidence is not limited to only subduction zones. The M_w 7.9 Izmit earthquakes were also preceded by 44 minutes of slow earthquake activity characterized by long-period signals that increased until the mainshock (Bouchon et al., 2011). The most enigmatic example would be the transition of a VLFE into an Mw 3.7 earthquake in a strike-slip setting in Alaska (Tape et al., 2018). The fact that these transition slip behaviors can occur in the same part of the fault interface as regular earthquakes raise questions about the mechanism that transforms one type of slip behavior to another. The 2011 Tohoku earthquake ruptured a part of the fault which previously associated with VLFE activity (Ide, Shelly, et al., 2007), raising questions about reassessing our understanding of basic fault mechanics, i.e., how fault interface and its material behave with different times and conditions?

VLFEs, LFEs, and TT are often associated with SSEs in the sense that if an SSE front passes through an asperity with favorable mechanical properties, it may produce one of these signals. In some tectonic settings, VLFEs and tremors have been seen to occur simultaneously, but sometimes they do not, even in the same area (Hutchison & Ghosh, 2016). Although we are just beginning to explore this spectrum of seismic signatures, it must be noted that much more observations and data are still required to explain this phenom thoroughly.

1.6 Methods of detection of Slow earthquakes

VLFEs and tremors do not have distinguishable P- or S- wave arrivals; hence they are more challenging to detect. Tremors typically emerge slowly from the background

noise and lack any exact seismic signature. The amplitude peaks at random during the episode, and their lack of easily identifiable features makes it difficult to distinguish them from cultural or environmental noise (Rubin 2011). the lack of an easily identifiable seismogram also contributes to the difficulty in locating TT. Several methods used in this dissertation include Beam-back projection, a grid-search centroid moment inversion, and matched filtering. The following is a brief introduction to each of these location methods.

1.7 Beamforming

Beamforming is a method applied across many types of physics. This method relies on generating a vector representing the timing for which energy in a specific frequency band arrives at each detection instrument within an array. In other words, the time and rate at which the signal reaches each instrument can give us a sense of direction and magnitude, which in seismology is slowness.

Beamforming is essentially summing the energy of the seismograms' vector space. In a coherent source, beamforming will produce constructive interference and destructive interference for noise. The beams will be more focused on a coherent signal or an NVT. The slowness vector is the inverse of velocity, and it is a way to represent the wavefront that accurately captures the order in which the instrument receives the signal from the source (Figure 1.2). A shallowly sloping wavefront, or low slowness, corresponds to a high-velocity source (high angle to Earth's surface). Thus, a high-velocity source is represented by a low slowness value. High-velocity sources indicate a deeper source since velocity increase with depth in the crust. When identifying slow earthquakes, they must have low slowness values since they tend t have source locations at the bottom of the locked

seismogenic zone. Lower velocities tend to correspond to shallower portions of the crust. Since beamforming can be used as an independent constraint to depth, it can help determine the relative depth of an event without relying on a velocity model. This helps rule out events that may appear like tremors in a seismogram but are anthropogenic noise sourced at the surface. For an exact location based on beamforming, beam back-projection uses the vector obtained in the slowness space and projects it onto a fault model. The fault model is created based on a local velocity model and is used to locate these events (Ghosh et al., 2009; 2012). Since beam back-projection relies both on the fault model and velocity model, it incorporates some errors based on the accuracy of the fault and velocity model. Multi-beam back-projection (MBBP) utilizes the same basics but uses multiple arrays. The error due to the velocity and fault model is eradicated since this method does not require either one. However, the availability of well-designed arrays is often poor. It can be highly accurate, but given the requirements for implementation, it is more challenging to implement. [Ghosh et al., 2009; 2012].

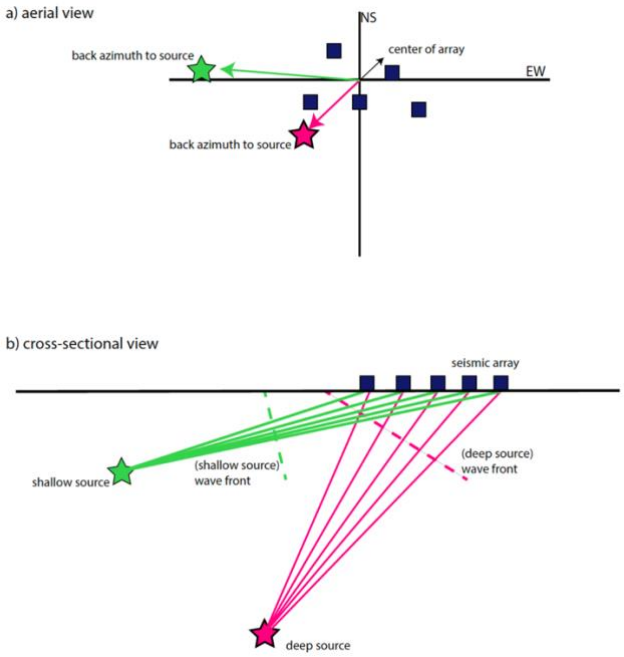

Figure 1.2: This is a schematic diagram of the way beamforming works. Two sources are given (one with a green star and one with a pink star, stations are displayed by navy blue squares). a) Gives an aerial perspective of how energy from a source will hit stations of an array in a particular order such that a back azimuth between the center of the array and the source can be produced. b) Gives a cross-sectional perspective of how a relative sense of depth can be determined through beamforming. Deep sources (pink) will have a shallow sloping wave front, and thus a lower slowness; shallower source (green) will have a steeper wave front, and thus a higher slowness. Shallower wave fronts (and low slowness) correspond to higher velocity sources, which correlate with greater depths. Steeper wave fronts have high slowness values and correspond to low velocity sources, which typically correspond to source locations that are shallower in the crust.

1.8 Grid Search Centroid Moment Tensor Inversion

Centroid Moment tensor inversion is based on the relationship between six zeroth order basis moment tensor of the earthquake source and the elastic vibrations associated with the earthquakes itself. Hence a seismogram $s_z(t)$ recorded at a station z, can be expressed as convolution of a of the Greens Function of the medium to an impulsive source G with a moment tensor element ‘n for source r decomposed into m elements.

$$s_z(t) = \sum_m G^s_{zm}(t) n^r_m ,$$

Here we divide our target area into 1km by 1km along latitude and longitude, 1km spacing along depth and assume that the source of the vent occurs at one of these grid points. By assuming a pure deviatoric tensor we can arrive at the following equation:

$$m = [G^T G]^{-1} G^T s ,$$

Here G is the kernel matrix comprising the Greens' function, s is the data vector and m consists of the six independent basis moment tensors.

Using the above equation and comparing the observed waveforms to the synthetic waveform at each grid point we can calculate the variance reduction which can be defined by the following relationship

$$V.R. = \left(1 - \frac{\sum_z \int (s_z(t) - o_z(t))^2 dt}{\sum_z \int (o_z(t))^2 dt}\right) \times 100 ,$$

Where sz(t) and oz(t) are the original and synthetic seismograms. Then we calculate the moment tensor for each of the grid point using a90 seconds sliding time wine and 1 s time step. The final solution is based on the V.R. and the percentage Compensated Linear vector Dipole (CLVD) which show the degree of similarity and residual radiation from the best double couple source model.

VLFEs have very low SNR in a low-frequency band. VLFEs have only 1-3 peaks and troughs, contributing to their detection and location difficulty. The most crucial part of this method boils down to generating synthetic seismograms. This process involves the convolution of a source-time function and a Green's function based on a 1-D velocity model of the study area. Further work is required to filter out actual events, but those criteria are discussed later in this dissertation.

1.9 Match Filtering

We use each detected VLFE event as a template to perform cross-correlation type matched filtered analysis applying a fast algorithm known as Super-Efficient Cross-correlation (SEC-C; Senobari et al., 2019). Each template event consists of 3 channel broadband data in the best moment tensor inversion solution. Each template is compared to continuous waveform data from the same respective stations and channels as the template event with a sliding time window. Time windows with values above a determined threshold value are cataloged as VLFEs. The threshold for a positive detection using noise templates must be done separately since the background noise would vary from region to region. Once the event passes through all the criteria, a catalog of events is created and reported to the user as a valid detection.

1.10 Summary of projects

This dissertation contains several studies that utilize slow earthquakes to determine more about the properties of the source area and slow earthquakes themselves. We have used multiple detection and location algorithms, reflecting the inherent difficulty of detecting these obscure events. These projects can delve into three areas. The first project focuses on discovering offshore VLFEs in the Cascadia subduction zone using ocean-bottom seismometers (OBSs). OBSs are notoriously noisy and very difficult to work with, especially when dealing with signals at VLFEs frequencies. However, with proper calibration and selection, OBSs can effectively detect and locate VLFEs. This study uses a grid-search moment tensor algorithm on OBSs to discover VLFEs offshore Cascadia. The fault structure in the offshore region is still unknown; however, this opens new avenues to

explore and observe these events. The VLFEs along the northern section near Vancouver Island have a focal mechanism that portrays largely thrust, due to subduction going in the area. However, the VLFEs, in offshore Washington and north Oregon seem to have major strike-slip faulting. Although no clear relationship could be seen between the ongoing onshore ETS, the discovery of VLFEs open a new avenue of fault stress release that has never been observed before in the offshore Cascadia subduction zone. Finally, a robust events catalog for VLFEs has been created, and further possible mechanism of these events are discussed. The second project focuses on discovering VLFEs in Taiwan (Chaudhuri and Ghosh, In prep) in the south-central range, which involves a grid search centroid moment tensor inversion algorithm (Ghosh et al., 2015; Hutchison & Ghosh, 2016). We were able to identify three distinct VLFEs in the south of the central range in Taiwan, and this was the first time we can see this form of seismic signature. We apply a matched filtered algorithm to create a robust VLFE catalog for three years, including a significant tremor episode time period. We show that the VLFEs repeat several hundred times over three years. The VLFEs in Taiwan also showed an exciting characteristic: they precede heightened earthquake activity in the area by 3-4 weeks. An empirical comparison of the event catalog and regional and local cataloged earthquakes revealed two such instances in this region and can be regarded as spatiotemporally related. The third project happened right around the corner at Cholame, California. Here we use beam back-projection to detect and locate just shallow and deep tremors to the south of the creeping section at Parkfield. The beam back-projection method consistently shows longer tremor duration than visual detection or the envelop cross-correlation method used in the Cascadia subduction zone

(Ghosh et al., 2009, 2012). We see hundreds of events, and this method provides a complete catalog compared to previously published ones. Results show that we detect more tremor activity than formerly known. We also see some shallow tremors (above 10 km) that have not been detected in this area before. Although shallow tremors have not been observed on the San Andreas Fault before, they have been seen in Japan. The occurrence of shallow LFE's also accompanies shallow tremors during these tremor episodes, and further analysis will tell us more about the physics of tremors in the region.

CHAPTER 2

Widespread Very Low Frequency Earthquakes (VLFEs) activity offshore Cascadia

Abstract

Cascadia subduction zone produces a wide variety of seismic events. A significant part of the stress in this subduction zone is released by Episodic tremor and slip (ETS) in the form of tremors, Low Frequency earthquakes (LFE), and onshore deep very low frequency earthquakes (VLFE) (Brown et al., 2009; Doran & Laske, 2017; Ghosh et al., 2015; Hutchison, 2020; Hutchison & Ghosh, 2016, 2019; Kao et al., 2010; Plourde et al., 2015). We discover widespread occurrence of multiple discrete VLFEs offshore Cascadia using ocean-bottom seismometers (OBS). They are the only seismic stress markers in this area so far, barring occasional regular fast earthquakes (Han et al., 2017; McGuire et al., 2018; Michel et al., 2019). Using centroid moment tensor inversion and matched filtered technique, we have detected, located, and studied sequences of 12 distinct VLFEs. The VLFEs along the northern section near Vancouver Island have a focal mechanism consistent with overall subduction zone deformation in the area. However, the VLFEs, along offshore Washington and north Oregon, seem to show strike-slip faulting, attributed to sediment consolidation, subduction bending, and transpressional regimes created by the complex plate tectonics in this area. The discovery of VLFEs opens a new avenue of studying fault stress evolution that has never been existed before offshore Cascadia subduction zone. We have created a robust catalog of VLFEs and explore their relationship to nearby seismicity and onshore deep tremor. They are an essential stress indicator for a future megathrust earthquake and a potential tsunami.

2.1 Introduction

Episodic tremor and slip (ETS) is defined by periodic intervals of slow slip along the plate interface and associate seismic radiation. The associated seismic events that comprise the ETS include nonvolcanic tremor and low-frequency earthquakes (LFEs) that emit seismic energy mainly in the 2-8Hz frequency bands but are depleted in energy in higher frequencies compared to regular fast earthquakes of similar magnitude. Studies at a number of plate boundaries have shown that tremors and LFEs coincide spatiotemporally (Brown et al., 2009; Shelly et al., 2007b; Sweet et al., 2014). Furthermore, tremor is likely LFE swarms resulting from shear slip during the slow slip occurring along major faults (Ghosh et al., 2009; Ghosh, Vidale, Sweet, Creager, Wech, Houston, et al., 2010; Li & Ghosh, 2017; Shelly et al., 2007a). Signatures of slow earthquakes are observed and/or inferred beyond the subduction zones (Hutchison & Ghosh, 2016; Mendoza et al., 2016; Nuyen & Schmidt, 2021; Takeo et al., 2010) and even used for structural studies (Huesca-Pérez & Ghosh, 2015). Very low-frequency earthquakes (VLFEs) are also responsible for a significant portion of the moment release during an ETS event (Ghosh et al., 2015; Kao et al., 2010). The moment released by VLFE activity during an ETS is typically greater than the cumulative tremor activity during the same time period (Ghosh et al., 2015). Although tremors in this area have been known to go on for weeks, a single Mw 3 VLFE releases an equivalent amount of moment (Kao et al., 2010). VLFEs have been debated as a bandpass signal of stacked LFEs (J. Gomberg et al., 2016; Ide, 2016) however, these two events often have an uncorrelated spatiotemporal relationship (Hutchison & Ghosh, 2016; 2019). VLFEs release much higher seismic moment than the other slow slip seismic events,

and hence their offshore presence in subduction settings can be very crucial in studying processes near the trench where tsunami may originate due to a large megathrust earthquake.

The Cascadia subduction zone (CSZ) extends from the Nootka fracture zone offshore British Columbia (Canada) in the north (Audet et al., 2008) to the Mendocino triple junction offshore northern California (USA). It results from the subduction of the Juan de Fuca and Gorda plates beneath the North American plate. Along and across strike variation in the tectonic geomorphology of the Cascadia margin result from complex interactions between these three plates (Han et al., 2018; McCaffrey et al., 2013; Nedimović et al., 2009; Watt & Brothers, 2020). The CSZ has been generally seismically inactive along the offshore trench area in terms of regular fast earthquakes, especially between the northern Nootka Fault and the southern Blanco fault. It is, however, a highly active place for ETS events and slow earthquakes (Ghosh et al., 2009, 2012, 2010a, 2010b; Gomberg et al., 2012; Kundu et al., 2016) downdip of the seismogenic zone.

VLFEs have been detected down-dip of the locked zone in Cascadia (Ghosh et al., 2015; Hutchison & Ghosh, 2016) and in other subduction zones around the globe, including both onshore and offshore Japan, (Baba et al., 2020; Ito et al., 2009; Kato et al., 2012), offshore Costa Rica (Walter et al., 2013), Ryukyu trench (Ando et al., 2012) and Guerrero, Mexico (Maury et al., 2016). It is critical to study VLFE activity to understand the role of these more elusive seismic events in the grander scheme of the slow earthquake spectrum in Cascadia. Many tremors and LFE imaging studies have revealed a near-constant along-strike migration pattern of tremors during an ETS event (e.g., Ghosh et al., 2010a).

Providing the relationship of these events with respect to the occurrence of VLFEs will help understand the physical processes behind these phenomena.

VLFEs and tremor has been observed to be spatiotemporally correlated in many studies including Japan (e.g., Hirose & Obara, 2010). Onshore VLFEs in Cascadia, however, occur with and without spatiotemporal correlation with tremor (Ghosh et al., 2015; Hutchison & Ghosh, 2016). They also occur quasi-continuously in time, even during inter-ETS time period. Offshore shallow VLFEs have been observed in Costa Rica (Walter et al., 2013), Japan (Nakano et al., 2018), and Ryukyu trench (Ando et al., 2012) .

2.2 Data

This study utilizes 3 component broadband data from the Cascadia Initiative (7D) network of Ocean bottom seismometers (OBS). The OBS stations used have been shown in Figure 2.1. The distribution of stations is chosen based on their proximity to the trench and good-quality continuous data availability.

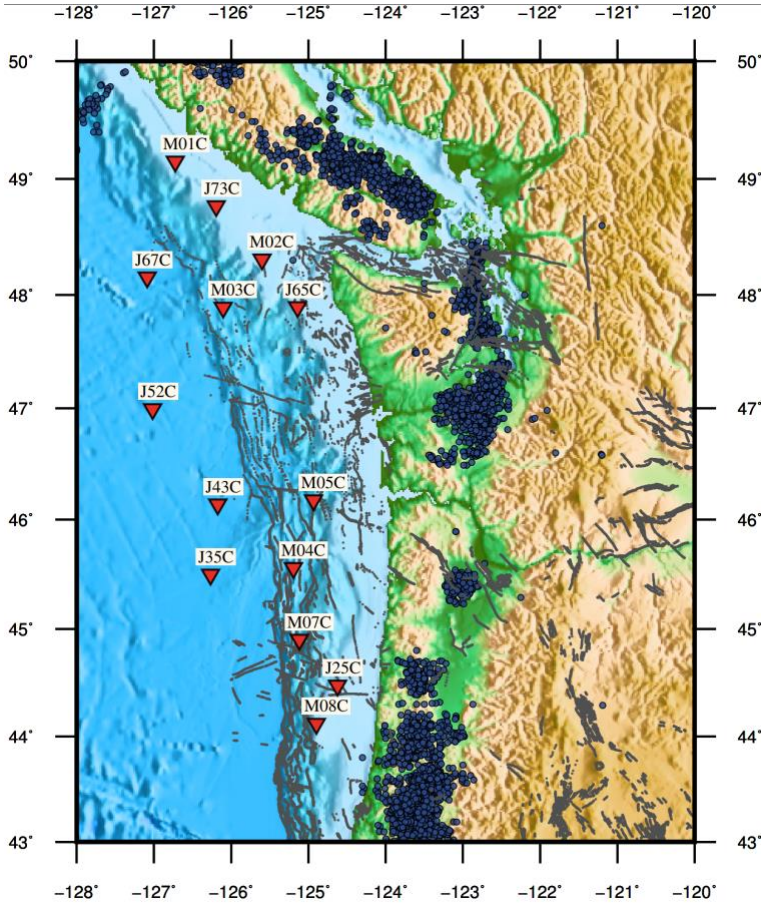

Figure 2.1: Study area in Cascadia subduction zone. Red triangles denote the OBS stations used here; gray lines indicate quaternary fault data obtained from United States Geological survey (https://www.usgs.gov/natural-hazards/earthquake-hazards/faults) and blue dots are the onshore tremor locations from the Pacific Northwest Seismograph Network (Ludwin, 2004; Wech, 2010)

A further data selection criterion based on the stability of their component orientation angle at higher cross-correlation values has been used. Seismic data from January 2014 to May 2014 was used for this study due to the availability of complete data during this time. To compare our findings (VLFEs) with ongoing tremor activity, this study uses an automatically generated tremor catalog from the Pacific Northwest Seismic Network (Ludwin, 2004; Wech, 2010). The time span is chosen to cover the time period

of the early 2014 ETS event and hence can be used to better compare the interaction, if any, among different types of slow events along the dip of the subduction fault. We have also used the offshore earthquake catalog (Stone et al., 2018) to compare the spatio-temporal relationship of VLFEs with regular earthquakes occurring in the vicinity. The location of these OBS stations covers offshore Cascadia along dip reasonably well – between the trench to the west and the coastline to the east.

2.3 Methodology

2.3.1 Channel orientation

Before analyzing the data, the OBS station channels' orientations need to be determined. Seismometers on land can be oriented accurately using gyro (Ekström & Busby, 2008; Ringler et al., 2013); however, determination of the orientation of free-fall OBSs is challenging. To precisely measure the orientation of the broadband channels (BH1 and BH2), we use the Doran Laske Orientation Python (DLOPy) module (Doran & Laske, 2017), which is based on measuring intermediate-period surface-wave arrival angles from cataloged teleseismic earthquakes from the Incorporated Research Institutions for Seismology (IRIS) database. This algorithm measures broadband surface wave arrival angles for individual teleseismic earthquakes. After selecting the events with the best cross-correlation values (> 0.8) for each azimuth, the algorithm determines the orientation of the horizontal components (Figure 2.2). Following correction of orientation for horizontal components, the instrument responses are removed and filtered in a bandwidth of 0.02-0.05 Hz, which has been observed to be the dominant frequency band for VLFEs.

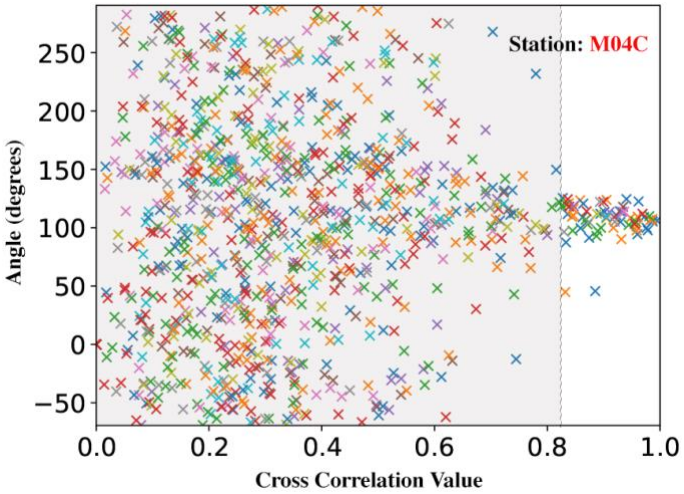

Figure 2.2: The above graph shows the output from the DLOPy orientation programs. The gray portion contains discarded events with correlation values less than 0.8, and the white section includes the selected events and the corresponding orientation

2.3.2 Centroid Moment tensor inversion

The study employs a grid search centroid moment tensor inversion method (CMTI). The study area stretched from 125° W to 127° W and 42° N to 47° N, and the grid is divided 0.1° by 0.1° horizontally and every 5km vertically. For detection and location, we use a strategy similar to Ghosh et al., 2015. Using a laterally homogeneous velocity model for the region, synthetic waveforms are calculated for each grid node at each station using a convolution of a delta function with the earth's structural response. Real (observed) broadband seismograms are compared to the synthetic (calculated) ones. Only the value with the highest variance reduction (V.R.) (i.e., the best match between real and synthetic seismograms) is recorded for each time window. VLFEs in Cascadia tend to have a signal duration of 90 seconds (Ghosh et al., 2015; Hutchison & Ghosh, 2016; 2019); hence we use a sliding time window of 90 seconds and recalculate the centroid moment tensor every

1s. The results include location, depth, strike, dip, rake, variance reduction, compensated linear vector dipole (CLVD), moment tensor, and focal mechanism (Figure 2.3).

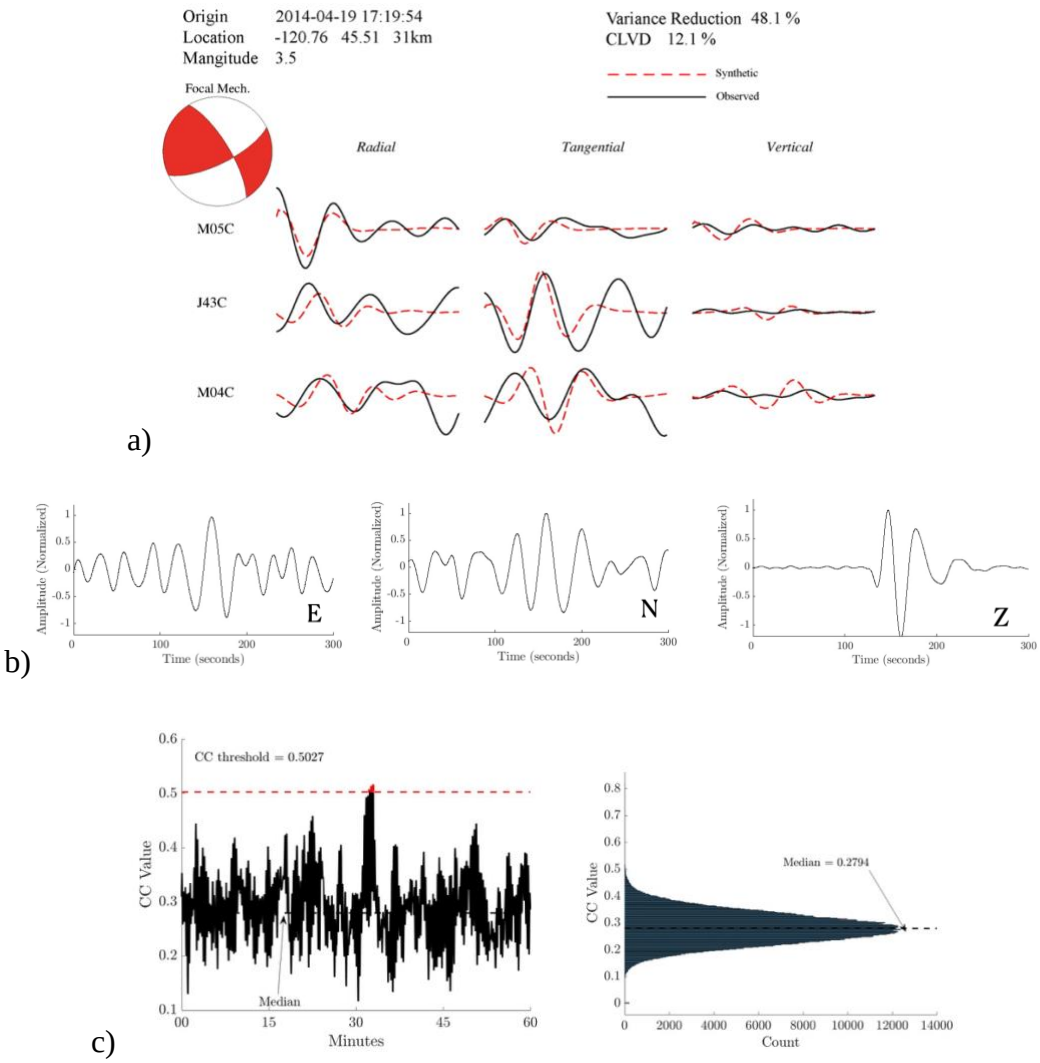

Figure 2.3: a) shows a detected VLFE offshore Cascadia using 3 OBS stations. The synthetic seismogram is denoted by the red dashed line, and solid black lines denote the observed seismogram. b) The figure shows three panels with stacked seismograms from the repeats of a detected VLFE. Stacking gives us a cleaner signal of the very low-frequency earthquakes, although individual events are often noisy. C) The left panel shows the cross-correlation threshold and the detection of an event in a hour long time period. The right panel shows the distribution of correlation value for the same day seismogram.

2.4 Results

2.4.1 Offshore VLFE distribution

We observe a total of 12 distinct VLFEs located offshore Cascadia, as shown in figure 2.4a. These are the first discrete offshore VLFEs observed in Cascadia, and they seem to repeat over a period of 5 months we have analyzed. Spatially, they cover ~550kms north-south, from northern Cascadia offshore Vancouver Island to central Oregon to the south. Along dip, they cover ~200 kms, between the trench and the coastline. Two distinct VLFEs along the northern section of the trench have a thrust focal mechanism with an average depth of 22 km, consistent with the area's geometry and depth of subduction fault. The central section offshore northern Oregon hosts 5 VLFEs with an average depth of 32 km, and the southern section offshore central Oregon shows 4 VLFEs with an average depth of 38 km. Although strict criterion has been applied to get a robust geographical location, the resolution in depth is not as robust due to the inherent limitations of the CMTI method. All the VLFEs along offshore Oregon have a primarily strike-slip focal mechanism with moment magnitudes ranging from 3.2 to 3.9, and their nodal planes are in close proximity with the existing upper plate mapped faults in the area (https://www.usgs.gov/natural-hazards/earthquake-hazards/faults). We do not find any obvious tremor signal during the distinct VLFEs.

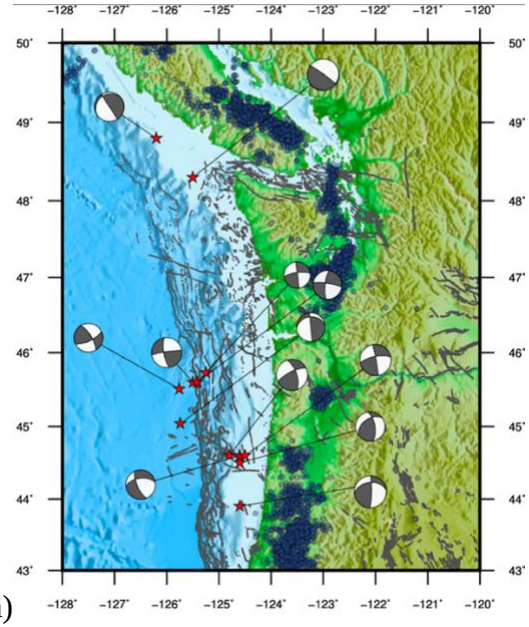

a)

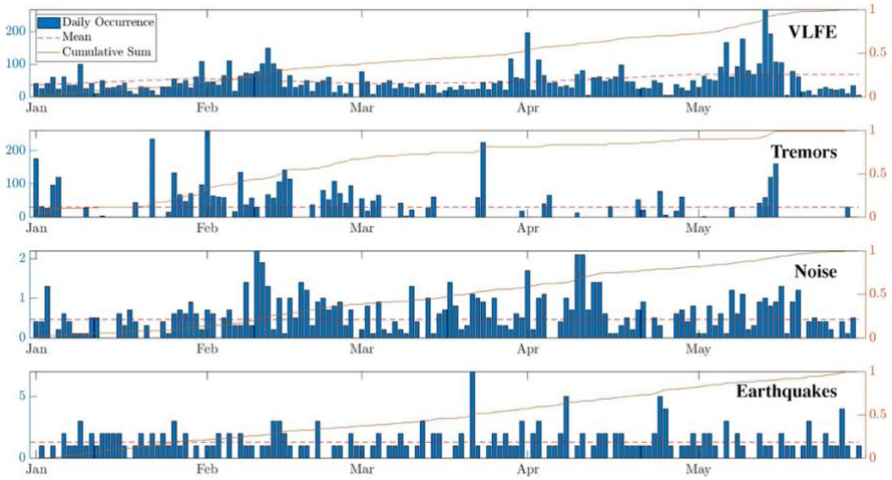

b)

Figure 2.4a) Red stars showing locations of 12 VLFEs and their focal mechanism along the offshore Cascadia subduction zone with blue dots representing the tremors from January to May 2014 (pnsn.org). The color shows the topography of the study area. B) Combined activity of slow and fast earthquakes. The top panel shows the combined VLFE activity of all 12 VLFEs. The second panel shows tremor activity onshore in the Cascadia Subduction zone. The third panel shows the noise activity in the area, and the bottom panel shows the earthquakes occurring in the region expanding from onshore to offshore Cascadia subduction zone.

We have considered the possibility that the VLFE signals detected by matched filter technique are noise, correlated with the template event just by chance. We have performed rigorous analyses to test this (Figure 2.4b). We use the match filtering technique to calculate the repeats of the VLFEs and compared them to background noise from random time windows of these stations. Please see section 2.3.3 for details. Our detection threshold is set to at least 1.5 times higher than that of background noise level with the same combination of stations. In other words, the detected VLFE signals are very unlikely to be random noise correlated with the template just by chance.

2.4.2 VLFEs, tremors, and Regular earthquakes

We compare VLFE distribution with an offshore regular fast earthquake catalog produced by Stone et al., 2018. We find an interesting spatial correlation of earthquake clusters with our VLFEs offshore Oregon (Figure 2.5). A cluster of VLFEs occur right at the edge of a cluster of regular fast earthquakes in map view. However, the earthquakes offshore Oregon do not show any obvious temporal coherence with the VLFEs during the 5 months of 2014 studied here. It is essential to understand that although stringent criterion has been applied to detect and locate VLFEs, a conservative estimate of VLFE activity has been obtained to provide robust results. More VLFEs in offshore Cascadia are likely occurring over the same time period but not detected for various reasons, like poor signal-to-noise ratio and limited broadband station coverage.

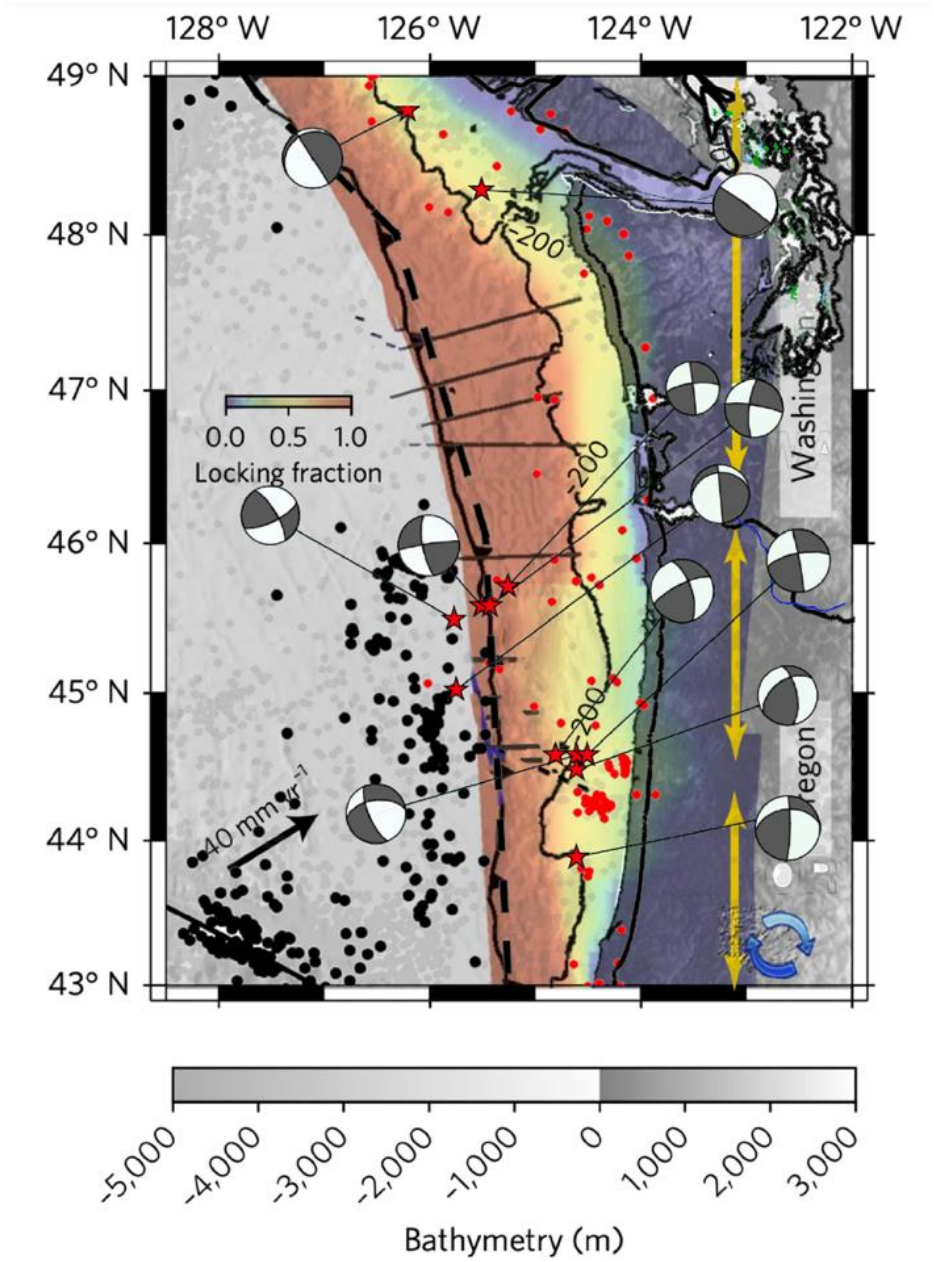

Figure 2.5: The above graph shows the locking fraction along the Cascadia subduction zone (Han et al., 2017; Schmalzle et al., 2014). Black dots represent regular fast earthquakes detected to the west of the Cascadia deformation front, and red dots indicate the earthquakes near and adjacent to the megathrust as cataloged by Stone et al., 2018. Contours show the depth of the Juan de Fuca plate at 10, 20, and 30 km (McCrory et al., 2012).

2.5 Discussion

Our analysis has revealed the existence of 12 distinct VLFEs along offshore CSZ. We observe a widespread occurrence of offshore VLFEs even in the short timespan analyzed. The VLFEs are mainly clustered offshore and near the trench area. These VLFEs are a vital stress marker considering the lack of regular fast micro-earthquakes in this area. The presence of offshore VLFEs in the CSZ clearly indicates that a significant amount of stress is released by these slowly slipping events that are not taken into account so far. CSZ has been tranquil, with only a few instrumentally recorded micro-earthquakes on the plate interface. However, paleoseismic studies indicate that this margin has hosted ~M_w 9 megathrust earthquakes at 200-500yr intervals with persistent rupture segment boundaries (Adams, 1990; Atwater, 1987; Goldfinger et al., 2012).

The 2 VLFEs along the northern CSZ show a thrust focal mechanism and are consistent with the overall plate tectonic setting in the area. However, the VLFEs along offshore Oregon within 43N and 46N show a primarily strike-slip motion, and these are distributed in the Siletzia terrain, offshore central Oregon of the CSZ. This area is characterized by reduced inter-seismic uplift and co-seismic subsidence, suggesting that a significant portion of the plate convergence is taken up by aseismic slip (Burgette et al., 2009; McCaffrey et al., 2013; Schmalzle et al., 2014). It is plausible that the VLFEs here play an important role in the total slip budget. The general lack of regular fast seismicity in this area also supports this idea. This reduction in seismic activity is further facilitated by the sediment consolidation at the subduction boundary. In this part of the subduction zone (between 43 N and 46N), under-consolidated fluid-rich sediments are subducting

beneath the forearc (MacKay, 1995; MacKay et al., 1992) and thus increasing the pore fluid pressure along the plate interface. This results in a variation in the locking fraction offshore North and central Oregon (McCrory et al., 2012) and creates a wider transition zone in the area (Schmalzle et al., 2014) which produces most of the VLFEs detected by this study.

Intriguingly, VLFEs along offshore Oregon show strike-slip mechanism. The presence of such strike-slip fault is attributed to the regional deformation of the submarine forearc and the oblique subduction of the Juan de Fuca plate (Goldfinger et al., 1997). An offshore cluster of regular earthquakes (Stone et al., 2018) and VLFE events in map view of central Cascadia are probably a manifestation of heterogenous frictional regime along this subduction zone. These events are likely due to a combination of transpression and crustal shortening in the overriding plate and convergence with an internally deforming and relatively young Gorda plate (Watt & Brothers, 2020).

Since tremors and VLFEs are often seen to occur downdip seismogenic zone in a warm subduction plate, the absence of tremors in the forearc indicates a highly locked portion of the subduction zone during the current inter-seismic period. In a natural subduction setting, the surface deformation after a great earthquake is controlled mainly by the slow deformation of the mantle wedge and the locking and slipping of the subduction fault. The deformation front along the CSZ has been observed to have faulting due to subduction bending (Nedimović et al., 2009),. In addition, offshore Oregon contains large offset faults that transect the oceanic crust and extend 6-7km into the uppermost mantle (Han et al., 2016). Exhumed subduction fault rocks have provided evidence for viscous

deformation of the matrix for which sediment is a major contributing component (relatively weak material) (Bebout & Penniston-Dorland, 2016). This suggests that ETS may arise from a combination of frictional and viscous behaviors (Fagereng & Den Hartog, 2017; Hayman & Lavier, 2014). The average P-wave velocity in this region also decreases as we move south towards offshore Northern Oregon, likely due to the enhanced porosity and alteration due to more extensive and through-crust faulting (Han et al., 2018). With subduction of a thicker sediment section (Kleinrock & Hey, 1989; Wilson, 1986), it is possible that the plate interface in these regions has fewer asperities and is more prone to aseismic sliding. Spatially adjacent clusters of fast and slow earthquakes (VLFEs) offshore Cascadia indicates coexistence of frictionally disparate fault patches, suggesting its multimodal nature of fault slip and stress release near the trench. The lack of regular earthquakes is partly compensated by these slow slipping events both along-strike and within the trench area of CSZ. Earlier studies revealed the deficit of regular earthquakes to compensate for the total amount of stress accommodated in this area. Recent studies in Japan (Baba et al., 2020; Nishikawa et al., 2019) showed that VLFEs, which were earlier thought to release stress only along downdip or updip seismogenic zone, often occur along the regular fast slipping region, i.e. the seismogenic zone. These VLFEs are likely indicators of interplate slow slip which compensates for the deficit in seismic moment are a result of pore fluid intrusion due to subducted seamounts (Nishikawa et al., 2019). Widespread occurrences of VLFEs along offshore Cascadia strongly indicates that slow earthquake plays an important role in accommodating deformation in this part of the subduction zone. It challenges a canonical view of a frictionally homogeneous seismogenic

zone bounded by transition zones on both up- and down-dip. Widespread activity of offshore VLFEs suggests a more heterogenous seismogenic zone capable of producing both slow and fast earthquakes. It is imperative to monitor and map out these events in details to have a clearer understanding of the earthquake deformation mechanism, seismic hazard, and seismotectonic processes in this area.

2.6 Conclusion

We discover widespread occurrence of VLFEs offshore Cascadia. This discovery suggests that seismogenic zone in Cascadia is far from our canonical view of a frictionally homogenous fault segment producing only regular fast earthquake. Instead, it is frictionally heterogenous with patches of slow earthquakes. This frictional heterogeneity of seismogenic zone may have important implications on the megathrust rupture and associated seismic hazard in this area. Offshore VLFEs likely contribute a significant amount to the total of moment release that had not been previously accounted for. The nature of stress release and its relationship with regular fast earthquakes is critical to understand the deformation processes in this region that experiences M9 earthquake. This study shows that slow slip maybe occurring along the Cascadia subduction margin offshore, which is fully to partially locked, preparing for the next large earthquake. Almost daily VLFE activity indicates that they play a major role in the stress release and deformation in this part of the subduction zone. These events may provide a critical understanding of the earthquake source and fault structure near the trench where megathrust earthquakes produce significant slip and damaging tsunamis. Offshore VLFEs maybe our best bet to study deformation processes near the trench where regular micro-

seismic activity is low. The Discovery of VLFEs in offshore Cascadia opens up new avenues to explore mechanisms controlling slow earthquakes, frictional properties along the entire Cascadia subduction fault including seismogenic and transition zone, and the physics of fault motion. More detail study covering a longer time span is needed to better characterize VLFE activities offshore Cascadia.

CHAPTER 3

Repeating Very Low frequency earthquakes modulate regular Fast earthquakes at the Central Range in Taiwan

Abstract

Slow earthquakes in the form of tremors and LFEs occur along the south-central range of Taiwan (Aguiar et al., 2017; Chao et al., 2012; Tang et al., 2010). This study detects discrete very low frequency earthquakes (VLFEs) using a grid search moment tensor inversion algorithm (Ghosh et al., 2015; Hutchison & Ghosh, 2019). By applying a matched filtered technique, we have created a robust VLFE catalog for three years. The two VLFEs closer to the tremor-producing region show a temporal relationship, but the western VLFE is the most active among the three. Our VLFE catalog of high temporal resolution allows us to identify a significant increase in VLFE activities preceding earthquake swarms. An empirical comparison of the VLFE catalog with regional and local cataloged fast earthquakes reveals two such instances. We show that fluid migration from deeper to shallower crust explains this modulation of regular fast earthquakes by VLFEs.

3.1 Introduction

The island of Taiwan occupies a key position in plate tectonics. It is situated along the boundary of the Philippines and The Eurasian plate. This area is characterized by a range of seismic activity, including fast slip in the form of large earthquakes, slow slip in the form of tremors, and low frequency earthquakes (LFEs) occurring adjacent to the seismic zone (Aguiar et al., 2017; Chao et al., 2012; Chuang et al., 2014; Ide et al., 2015;

Tang et al., 2010). Both fast and slow slips likely interact and affect fault planes, including the seismogenic zone where most large, damaging earthquakes occur. These slow earthquakes tend to happen primarily downdip to the seismogenic zone from a depth of ~12 to 38 km (Tang et al., 2010). However, seismic signatures of slow earthquakes – tremors, LFEs, and very low frequency earthquakes (VLFEs) are challenging to detect. LFEs have been found in many places where tremors have been detected, including in Taiwan (Aguiar et al., 2017; Tang et al., 2010). Tremor is the most common form of a seismic signal associated with slow earthquakes. However, VLFEs remain elusive in many regions that experience slow earthquakes, including Taiwan. The most convincing evidence of VLFEs has come from the southwest Japan Subduction Zone, Ryoku trench, and Cascadia Subduction Zone (Ghosh et al., 2015; Hutchison & Ghosh, 2019; Matsuzawa et al., 2015; Nakano et al., 2018). Ide et al., 2015 showed the first evidence of very low frequency energy of slow earthquakes in Taiwan by stacking tremors windows. Although tremor signals often accompany VLF signals (e.g., Ide et al., 2008), we don't always observe the same in many areas including Cascadia (Hutchison & Ghosh, 2016). The activity of discrete VLFEs and their spatiotemporal distribution in Taiwan so far remain unknown. Here we find 3 families of VLFEs on the island of Taiwan which is asynchronous with the tremor activity in the area. These VLFEs repeat several hundred times during three years of observation. We detect and locate these VLFEs, estimate their source parameters by a moment tensor inversion method, analyze their spatio-temporal distribution relative to tremors and regular fast earthquakes, and explore implications on a possible connection between slow and fast earthquakes.

3.2 Data & Methods

3.2.1 Centroid Moment Tensor Inversion (CMTI)

We analyze three components of seismic data from eighteen broadband stations in Taiwan (Fig 1a) for April through June 2010 – a period of high tremor activity – to look for VLFEs. We applied a grid search moment tensor algorithm (Ito et al., 2009) to detect VLFEs and estimate their locations and moment tensors. We initially divide the study area into a 3-D grid with 0.1 degree horizontal spacing and 5 km vertical spacing. The grid covers a wide geographic area, including the tremor zone, and extends far beyond it in all directions, almost covering the entire island. We have done this to ensure that our results are not biased towards a particular location. After correcting for instrument response, we filter the displacement seismograms in 0.02 to 0.05 Hz and use 90 seconds sliding time window with a 1 second time-step to perform moment tensor inversion. We obtain a point source centroid moment tensor solution at each time step and grid node. We assumed an impulse function source and identified the solutions that maximize the variance reduction, which is a measure of the goodness of fit between observed and synthetic waveforms. Time periods with high variance reduction with respect to the background are selected to flag potential VLFEs. We remove windows with cataloged earthquakes and teleseismic or regional wave-trains. Finally, all station combinations are used, and only stable solutions with finer horizontal (0.025 degrees) and vertical resolution (1 km) are kept. Applying this method, we detect three unique VLFEs.

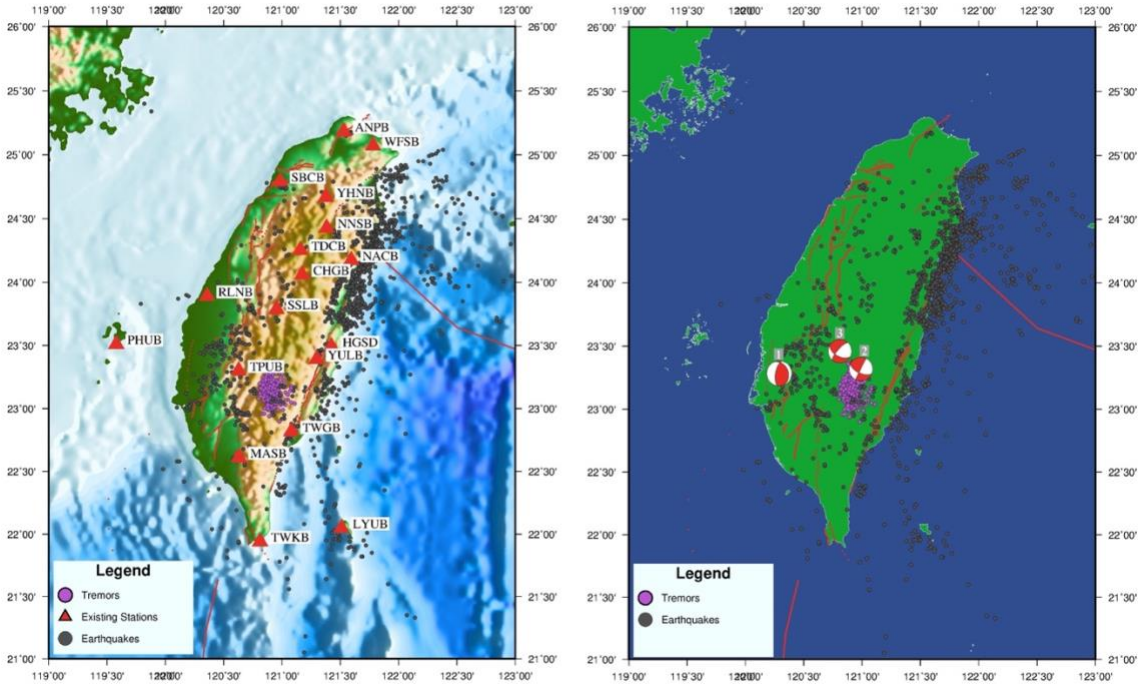

Figure 3.1: a) Map all the seismic stations (red triangles) in Taiwan with earthquakes (blue circles) and tremors (turquoise circles), b) Map shows the 3 detected VLFEs along with their focal mechanisms.

3.2.2 Matched Filtered Analysis

We perform cross-correlation-based matched filtered analysis applying a Super-Efficient Cross-correlation (SEC-C; Senobari et al., 2019) using the three VLFEs as templates. Each template event is generated using 3 component broadband data from the station included in the best moment tensor inversion solution. These templates are then compared to continuous waveform data from the same respective stations, with a sliding time window, to determine the cross-correlation coefficient. Time windows with values above a determined threshold are cataloged as VLFEs similar to the templates. In order to detect the repeats we use 5 times the mean absolute deviation (MAD) value added to the

median of the data as our threshold of detection (Shelly et al., 2007b). This threshold eliminates spurious noise signals to be picked as repeated events. (Figure 3.2)

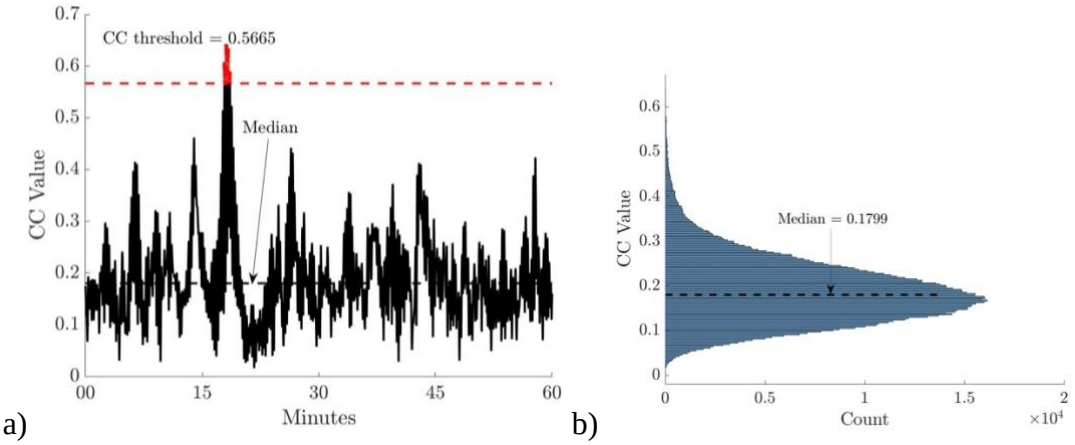

Figure 3.2: a) shows the cross-correlation threshold and the detection of an event in an hour-long time period. b) shows the distribution of correlation value for the same day seismogram.

We also perform an extensive cross-correlation analysis of background noise to minimize the effect of noise in the catalog and select a cross-correlation threshold. We select 100 random time windows that presumably consist of background noise because the template events did not detect them, and they do not contain any cataloged or visible seismic event. Using the station configuration for each template event, we create background noise catalogs for all 100 background noise time windows during the same time period. We then select our templates that repeat at least 1.5 times more than the average background noise. Once a catalog of matched filtered events is generated within a time period from January 2009 to December 2011, we stack the detections from each template for each channel (Figure 3.3b). This is done to increase the signal-to-noise ratio of these signals and show clear waveforms of repeating signals.

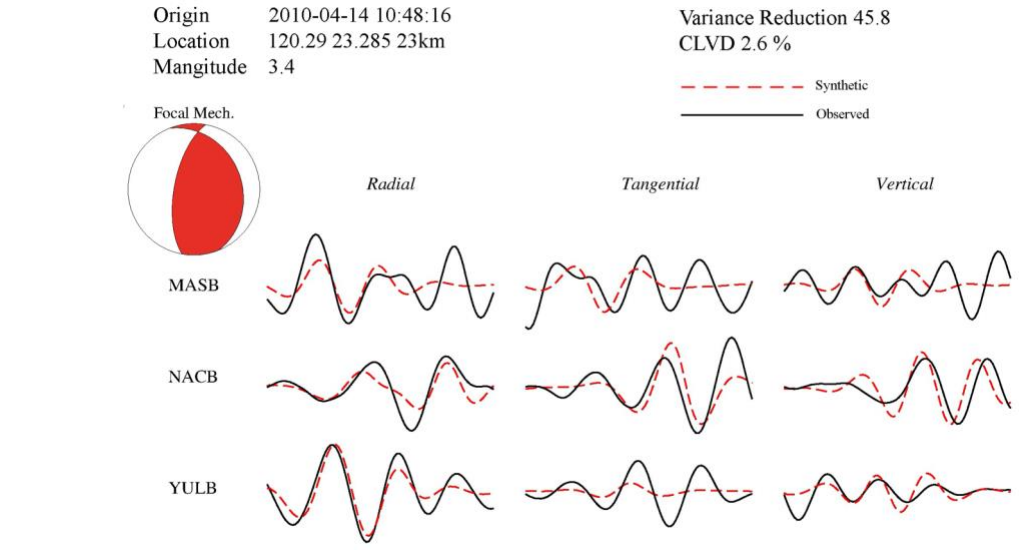

a)

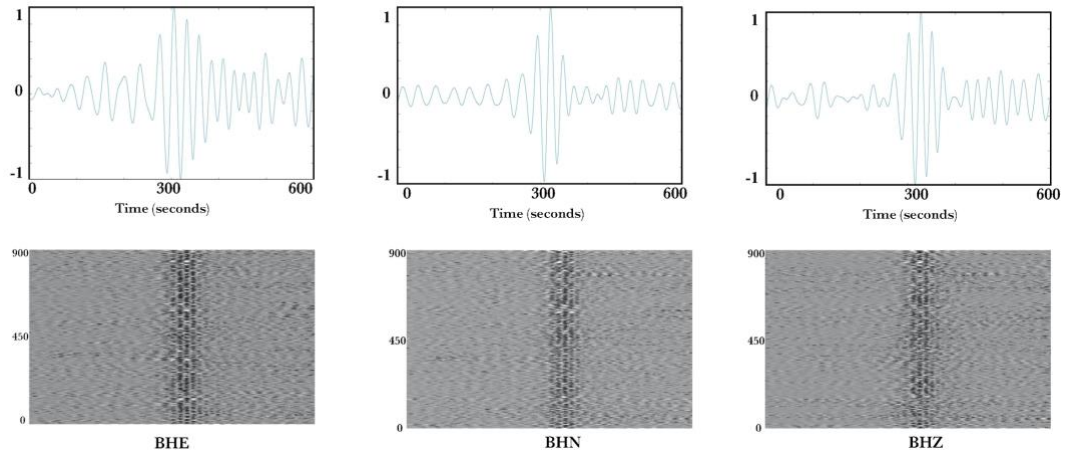

b)

Figure 3.3: a) an example of centroid moment tensor solution of the VLFE on the Chiayi fault. b) Shows stacked channels for all the repeats (limited to 900 recurrences) of the above VLFE.

3.3 Results

3.3.1 VLFEs and Their Temporal Coherency

Centroid moment tensor inversion allowed us to identify and detect three VLFEs with moment magnitudes of 3.4, 3.2, and 3.2 from west to east, respectively, on the

island of Taiwan. They are enriched in frequencies ranging between 0.02 and 0.05 Hz but are depleted in higher frequencies compared to regular local earthquakes of similar magnitude. Two of three VLFEs are located close to the tremor-producing region of the south-central range (Aguiar et al., 2017; Chao et al., 2012; Tang et al., 2010), which has a strike slip dominant focal mechanism. The other VLFE is located closer to the western edge of the continent on the Coastal Plains and has a primarily thrust mechanism, consistent with the tectonics in this area (Beyssac et al., 2007; Chen et al., 2019). The three VLFEs repeat ~700 times over three years, and this catalog excludes any possible events due to teleseismic or regional earthquakes. VLFE 1 along the western edge of the main thrust front is the most active VLFE with ~9 events/month compared to the VLFE 2 and 3 with ~4 events/month. The VLFE 1 originates from a depth of 25km with a variance reduction of ~46% (figure 3.3), which is similar to VLFEs found in other studies [e.g., Ghosh et al., 2015; Ito et al., 2009]. In contrast, the VLFEs along the central range comes from a slightly higher depth of 40km and 30km from west to east. Our method, however, does not have a good resolution in depth. These three VLFEs seem to have some temporal coherency with each other. Interestingly, the VLFEs along the central range seem to follow a more similar pattern compared to VLFE 1. The VLFEs (2 and 3) along the central range have a high temporal correlation with each other but do not seem to correlate with the tremor activity just south of it (Figure 3.4). This, combined with their difference in location with tremor, may imply that VLFEs and tremors occur on different families of faults or closely spaced uncoupled faults. However, the VLFE along the Southwestern range (on Coastal Plains)

shows a weaker temporal correlation and a different focal mechanism, which is consistent with the fact that it is clearly separated in space and located on a separate fault.

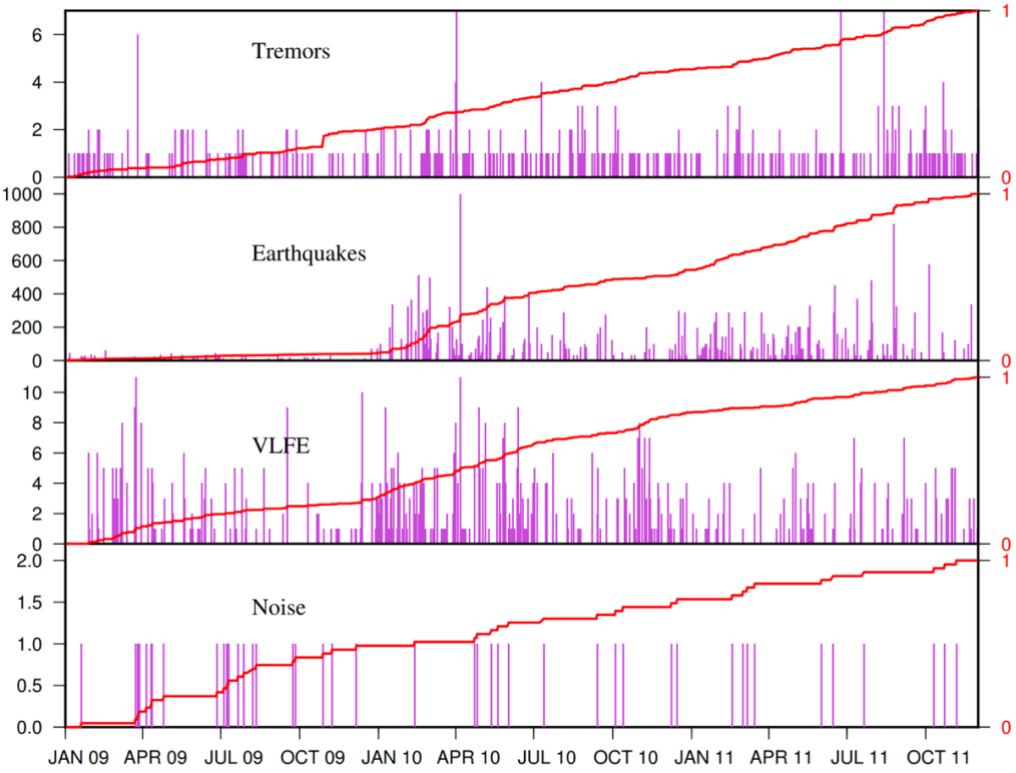

Figure 3.4: The top three panels show the number of daily occurrences of VLFEs (turquoise bars) and corresponding normalized cumulative plot (red) for the time span of 3 years from 2009 to 2011. The bottom panel shows an average of repeating noise templates, with station data from SSLB, YULB, and NACB from the whole time span with a mean of 0.05 events/day.

3.3.2 Spatio-temporal relationship of VLFEs to tremors and regular fast earthquakes

A regional earthquake catalog was obtained from the Broadband Array in Taiwan for Seismology (BATS) to compare its spatio-temporal variation with the VLFEs. We narrowed our catalog to contain only regional earthquakes within a radius of 1 to 1.5 degrees to contain all the three VLFEs. We compared the VLFEs with the earthquakes

around them. We also ensured that we do not include any earthquake mainshock and aftershock sequence. It can be clearly seen that there is a temporal relationship in January 2010, and this was followed by activation of tremors in the south-central range of Taiwan (Figure 3.5 and Figure 3.6)

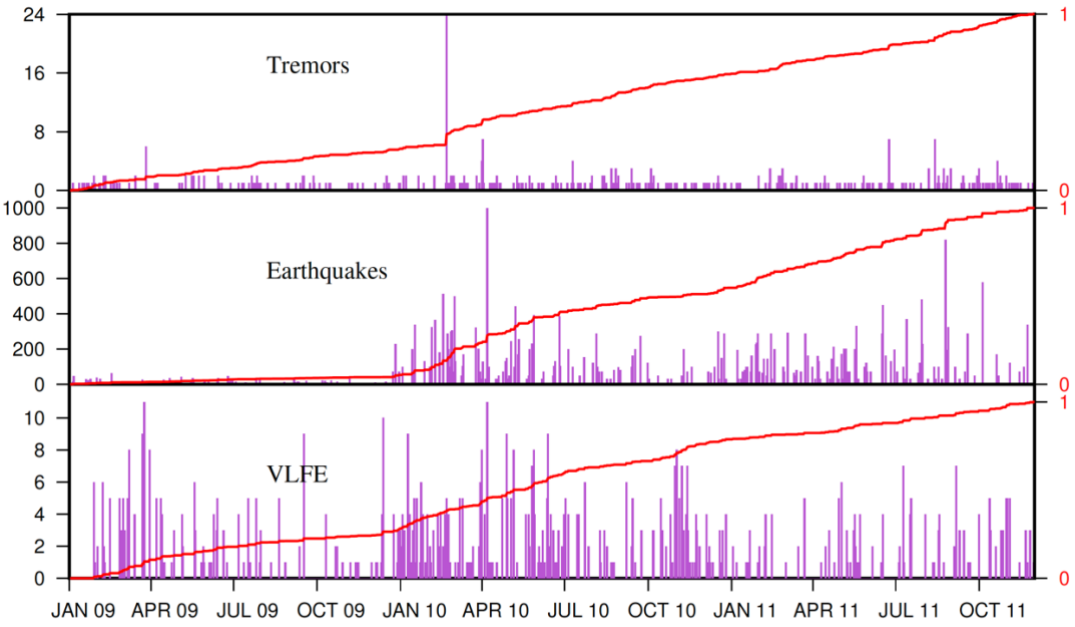

Figure 3.5: The daily occurrence frequency of VLFEs (combined activity), Earthquakes, and tremors in turquoise bars and the normalized cumulative plot (red) for the time span of 3 years from 2009 to 2011.

We found that an increase in rate of VLFE is followed by an increase in rate of regular earthquake nearby. This is clear after we combined the daily frequency of all the VLFEs. The daily mean increased ~ 3.2 times (from 0.52 to 1.63 events per day) in January 2010. Another heightened VLFE activity, with an increase in daily mean of ~2.8 times (from 0.53 to 1.49 events per day), is also observed in November 2010. A delayed heightened earthquake activity followed both episodes. Two clear instances of temporal relationship can be observed in the time span of 3 years. It appears that earthquake swarms

follow heightened VLFE activity in this region. In both these instances, the time lag between increased VLFEs and regular earthquake activity is approximately 3-4 weeks (Figure 5b and 5c). We infer that this is caused by delayed transfer of stress from the deeper to the shallow seismogenic crust. Since all the events were selected under stringent selection criteria, likelihood of background noise creeping into detection is small. The VLFEs, although occurring likely on different faults, still tend to influence behavior and activity of seismogenic crust nearby. We do not see an obvious temporal relationship between VLFE and tremor, although they are located nearby.

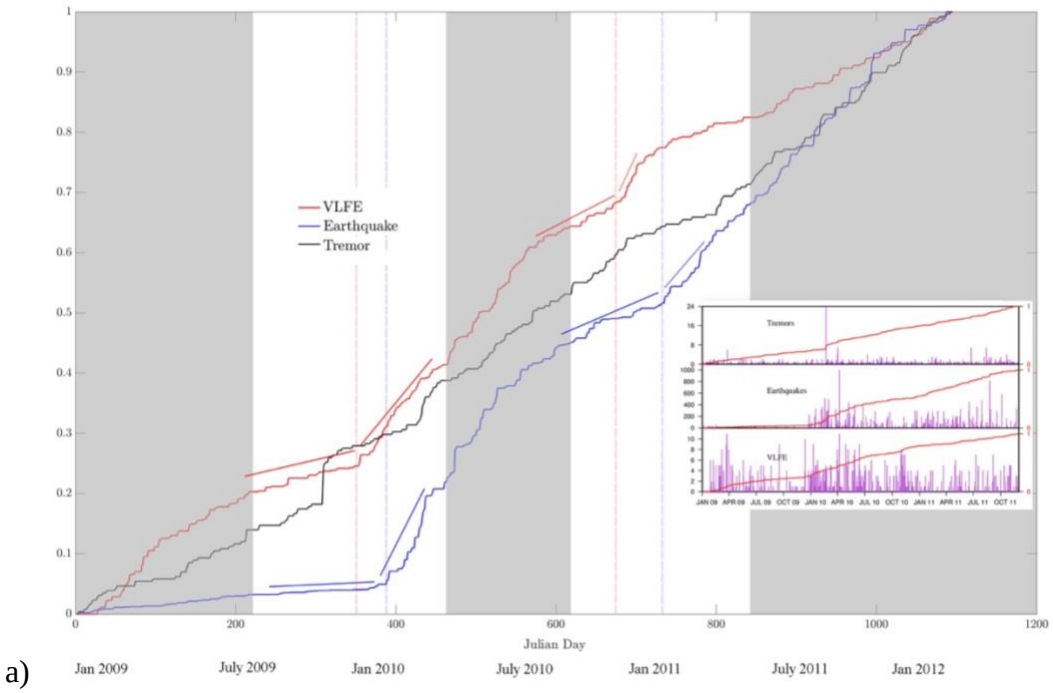

Figure 3.6: a) shows the change in activity for the three events from January 2009 through December 2011. The change in slope of the VLFE activity is followed by an earthquake activity in 2 instances in January 2010 and November 2010. The mean of VLFE activity (averaged over a month) changes from 0.7 to 1.2 during both times. B) & c) Highlights these two events and shows the change clearly and delayed triggering of earthquake activity in a time span of ~3-4 weeks

3.4 Discussion and Conclusion

Slow slip in the form of tremors has been observed in Taiwan to occur around the location of a major earthquake (C. H. Lin, 2012; W. Peng et al., 2019). Ide et al., 2015 use

centroid moment tensor inversion on stacked tremor seismograms and identified energy in the VLF spectrum. These tremor windows were proposed to be always concurrent with VLFEs in Taiwan (Ide et al., 2008, 2015). However, with the discovery of discretely identifiable VLFEs, we observe additional interesting connections between slow and fast earthquakes. Our analyses in this study indicate that heightened activity of these deep events leads to the regional shallow earthquake swarms observed in the area. However, temporal relationship between VLFE and tremors activity remain unclear. VLFEs are relatively deep events, and their activity presumably loads the shallower seismogenic crust (Rogers & Dragert, 2003). The Taiwan foreland basin, to the east of the thrust front, is highly active. This activity is often attributed to the presence of yielding over thrusted lower crust on the upper crust (A. T. Lin & Watts, 2002; Yeh et al., 1998). The observed spatio-temporal pattern indicates that the VLFEs at the base of the fault is likely influencing the seismic activity in the seismogenic crust updip.

In many areas, including Japan (Kato et al., 2012) and Chile (Ruiz et al., 2014), slow slipping seismic and geodetic events have been observed. They have been attributed to stress transfer from deeper part of slowly slipping fault to the shallower seismogenic crust. We propose that VLFEs in Taiwan modulating regular earthquakes due to fluid flux from deeper (wet) part of the fault to shallower seismogenic crust (Gurevich et al., 2010; Husen & Kissling, 2002; Nakajima et al., 2013; Nippress & Rietbrock, 2007; Sibson, 2013). As suggested by Chuang et al., 2014, the area of these slow events are characterized by metamorphic dehydration and the eventual extension forcing the release of fluid. We infer those subsequent migrations of fluid into the shallower seismogenic crust triggers

faults and modulate regular seismicity in this region. Here we use a lower crustal diffusivity (D) of ~4m^2s^{-1} (Warner, 2004) and the fluid diffusion curve of $r = \sqrt{4\pi Dt}$ (Shapiro et al., 1997), where r and t are the distance and time relative to the main event (VLFE). We estimate a time difference of 23-51 days for depth ranging from 10-15 km and this is consistent with our observation of the delay. A surge of VLFEs likely indicates a relatively larger slow earthquakes in a region with high pore fluid pressure in the base of the fault. The time lag of 3-4 weeks probably reflects the time required for fluids to migrate 5-10 km upwards and eventually bring the system to brittle failure. Similar mechanisms have been proposed to explain episodic tremor and slip in Cascadia (Audet et al., 2009).

Slow seismic earthquakes (tremors, LFEs and VLFEs) release a tiny fraction of the total geodetic moment (Kao et al., 2010). However, the total moment released by a week of tremor is approximately equivalent to the moment released by a single VLFE event of Mw ~3. The discovery of VLFEs in Taiwan suggests that these events also contribute significantly to the total moment released by slow earthquakes in this area. While tremors have their maximum energy in the higher frequency range of slow seismic expression, VLFEs mostly stay in the lower part of the spectrum. Although few instances of strong bursts of tremors are associated with heightened VLFE activity, many strong tremors and VLFE bursts are not correlated. Therefore, whether tremor and VLFEs represent different parts of the frequency spectrum of the same slow seismic event remains an open question. VLFEs in Taiwan show that a significant amount of seismic moment released by these events had not been accounted for previously. The nature of slow earthquakes in this region is more complex than presented in earlier studies. Careful observation of the temporal

occurrences of these events reveals a relationship between regular earthquakes and VLFEs, which is important to understand how different parts of the fault behave and interact.

It is important to understand that although strict criterion has been applied to detect and locate VLFEs, a conservative estimate of VLFE activity has been obtained to maintain robust results. More VLFEs in Taiwan are likely occurring over the same time period but not detected for various reasons, like poor signal-to-noise ratio and limited broadband station coverage. Regardless of undetected events, VLFEs constitute a vital part of the seismic signature of slow earthquakes and present an opportunity to study their source physics. The Discovery of VLFEs in Taiwan opens up new avenues to study mechanisms controlling slow earthquakes, frictional properties in the transition zone, and the physics of fault motion.

3.5 Acknowledgement

Thank you to Kevin Chao who have provided useful and complementary insights into this investigation and the tremor catalog for this study area (https://www.kevinchao.com/tremor-catalogs). The broadband data used in this study came from Broadband Array in Taiwan for Seismology (https://bats.earth.sinica.edu.tw/).

CHAPTER 4

Complete imaging of tremors and their interaction with other slow and fast earthquakes in San Andreas fault – their implications in fault dynamics and seismic hazard

Abstract

The San Andreas Fault (SAF), a right lateral strike slip fault, is one of the most micro-seismically active and well-studied faults. However, a new phenomenon of slow earthquakes and tremors has been observed recently near Cholame and Parkfield (Nadeau & Dolenc, 2005). Earlier reports of tremors from this area were given by many scientists but the sensitivity and level of detection is not as robust as that of the beam back projection technique. Getting a clearer picture about the interaction of slow and fast earthquakes, the dynamics of slow earthquakes, their mode of migration, dynamic triggering and their spatiotemporal variability are key targets to this project. In this project, I use a mini seismic array near Cholame to image tremor in high resolution along SAF. A mini seismic array along with beam back projection technique detect 5 times more tremor activity compared to conventional methods (Ghosh, Vidale, Sweet, Creager, Wech, Houston, et al., 2010; Li & Ghosh, 2017) tracking its activity continuously. The higher sensitivity and resolution of our array will provide us with new information about the underlying physics behind the cause of slow earthquakes. Understanding how the activity of tremors and LFE's would perturb the behavior of fast/damaging earthquakes is important for earthquake hazard and safety. Results show that we detect more tremor activity than previously known. We also see some shallow tremors (above 10 km) that have not been detected in this area before.

Although shallow tremors have not been observed in San Andreas Fault before, they have been observed in Japan. The presence of possible shallow tremors is also accompanied by the occurrence of shallow LFE's during these tremor episodes, and further analysis will tell us more about the physics of tremors in the region. The data has been used to systematically detect and locate LFEs and find their interaction with various other slip events.

4.1 Introduction

Plate tectonics leads to the accumulation of stresses at the plate boundaries. These stresses are released by fast earthquakes and slow earthquakes, which include tremors, LFEs, and VLFEs. These slow earthquakes release some stress, and they provide valuable sub-crustal information otherwise unavailable. The physical mechanisms governing non-volcanic tremor (NVT) and LFEs, which have been observed in subduction zones and the strike-slip environment globally, remain unclear. Tremors are identified by the increased amplitude of coherent signals recorded in multiple stations. They can be distinguished from background noise, having a higher coherency and amplitude across the array and a lower slowness(Ghosh, Vidale, Sweet, Creager, Wech, & Houston, 2010; Ghosh, Vidale, Sweet, Creager, Wech, Houston, et al., 2010). In subduction zones, they last from minutes to hours to days and have a dominant frequency range of 2-10 Hz. Due to the absence of indistinguishable impulsive body waves, it is sometimes difficult to locate them using conventional methods. The most used method of tremor location is based on envelope cross-correlation of seismic traces (Nadeau & Dolenc, 2005; Obara, 2002; Rubinstein et al., 2009). Tremors have also been analyzed using seismic array techniques (Fletcher &

Baker, 2010; Ghosh, Vidale, Sweet, Creager, Wech, Houston, et al., 2010; La Rocca et al., 2005, 2008, 2010). In addition to tremors, array methods have been extensively used to understand different seismic sources and the earth's structure in seismology.

The SAF in central California has a complex frictional behavior at depth discernable by the change of the creeping Northwest portion to the locked Southeast portion, which was last ruptured in the 1857 Mw 7.8 Fort Tejon earthquake (Sieh, 1978). Based on the analysis of continuous recordings from the borehole High-Resolution Seismic Network (HRSN) and surface stations in the Southern California Seismic Network (SCSN), Nadeau & Dolenc, 2005 found clear evidence of tremor around the SAF near Cholame south of Parkfield. The inferred hypocentral region coincided with the epicenter of the 1857 Mw 7.8 Fort Tejon earthquake (Sieh, 1978). The tremor found near Cholame appears to be analogous in terms of depth, frequency content, polarization direction, and dominance of shear waves found around the circum-Pacific subduction zones (Obara, 2002; Rogers & Dragert, 2003; Schwartz & Rokosky, 2007). However, the SAF tremor is less frequent, with a shorter duration and smaller amplitude (Nadeau & Dolenc, 2005). Shelly et al., 2009 calculated precise locations of LFEs near Cholame and showed near-linear features parallel to SAF strike near the fault's surface trace but located below the seismogenic zone. This suggests that at least a portion of the tremors occurs on the deep extension of the fault and likely represents sheer slip, like those found at other subduction zones (Shelly et al., 2007a, 2007b). Gomberg et al., 2008 discovered tremors triggered by the 2002 Mw 7.8 Denali Fault earthquake at seven locations and the entire SAF system in California, with two in central California. Z. Peng et al., 2008 analyzed these two tremor

sources triggered by the Denali Fault earthquake in detail and found that they originated near the base of the seismogenic zone along the SAF. The tremor was excited when the Love waves impart right-lateral shear stress and boost slip on the SAF. Ghosh et al., 2009 found similar results for the tremor triggered by the 2004 Mw 9.2 Sumatra earthquake and tremors associated with the passage of teleseismic P waves. They strongly suggested that dilatational stress may also be significant in triggering tremors. However, shallow tremor occurring in or above the seismogenic zone remains elusive in SAF.

Fault shows a variety of slip behaviors to accommodate significant amounts of stress. The major ones observed in many plate boundary faults are slow and fast earthquakes. How they interplay to govern the tectonic behavior of faults and physical processes controlling them remains enigmatic. The San Andreas Fault (SAF) near Cholame is a perfect place to study these phenomena because it produces plenty of regular seismicity (fast earthquakes) as well as slow earthquakes (tremor, low frequency earthquakes). Previous studies (Guilhem & Nadeau, 2012; Shelly, 2017) in this area provide an idea of the spatiotemporal distribution of tremor and low-frequency earthquakes (LFEs). However, the method employed only allows a low resolution or spatially incomplete detection and imaging of slow earthquakes, providing us a fractional picture of the slow earthquake dynamics in this area. This project uses an array technique (Ghosh et al., 2009, 2012) to image tremor in high spatiotemporal resolution detecting five times more tremor activity duration than a conventional envelope cross-correlation (ECC) method. In addition, preliminary results show multiple solid lines of evidence of shallow tremor and LFEs in the seismogenic zone. This study will produce a comprehensive tremor catalog for

this area for the year 2013 using continuous seismic data we collected by a well-designed mini seismic array. This work will provide a better and more complete understanding of the spatiotemporal distribution of tremor and LFEs, their possible relationship with regular fast earthquakes. The higher detection combined with spatial and temporal variability help detect new patterns of migration, their primary stress evolution in the deeper and shallower crust, and how they might relate to regular earthquakes, especially for tremors in the shallow seismogenic crust. Although not the scope of this work, the catalog can be used to get an insight into the dynamic stress threshold, partitioning of stress release between fast and slow modes of slip, helping us better evaluate seismic hazards of this area and in other areas with a broad spectrum of fault slip.

4.2 Data

The array consists of 18 broadband seismic stations (Figure 4.1). They have been continuously recording seismic data since April 14, 2013. Ghosh Earthquake Seismology Lab had installed the mini array at the UCR has been running continuously for about four years. Each station is equipped with a Nanometrics Compact Trillium sensor with a flat response to 120 sec. In addition, we use a Taurus datalogger, solar panel, and GPS clock. The array is designed to image signals between 20 Hz and 10s of seconds but optimized explicitly for the signal between 1 and 15 Hz (i.e., the tremor/LFE band).

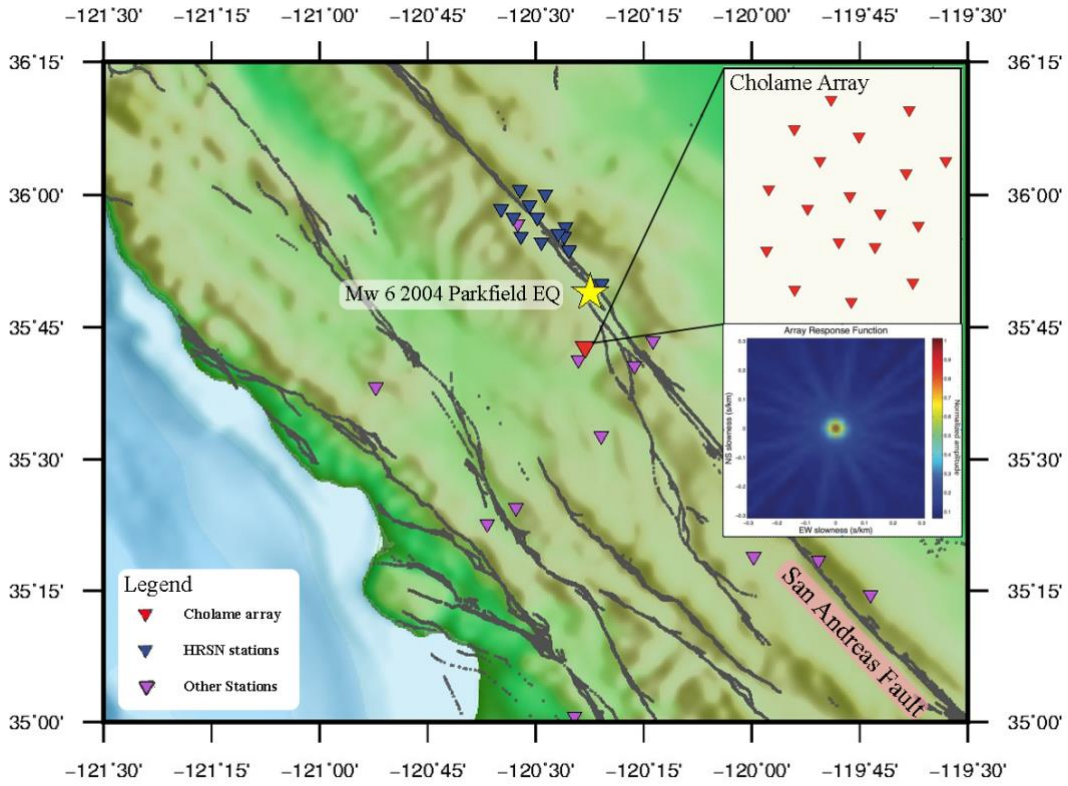

Figure 4.1: Map of the San Andreas Fault along with the Cholame Array (marked as CW), The 2004 Parkfield Earthquake and the Monarch peak. Top Inset: Shows the station configuration of the Cholame array and the bottom inset shows Array response function at 10 Hz for the Cholame West (CW) Array. Note the peaked response indicating a very high resolution obtained by the array.

It is strategically located near Cholame to maximize tremor and LFE detection located in the SAF with exemplary geometrical configuration. The array response function shows an excellent peaked and coherent response at 10 Hz (Figure 4.1), indicating that the array can efficiently resolve low amplitude seismic signal even at 10 Hz very clearly (lower frequencies are even better). Such an array response function makes it suitable for imaging

tremor, LFE, and regular earthquakes with high precision with an enhanced signal-to-noise ratio.

4.3 Methodology

We apply the beamforming method to scan the continuous seismic data collected by mini arrays automatically. The beam back-projection method consistently shows higher tremor duration than visual detection or the envelop cross-correlation method used in the Cascadia subduction zone (Ghosh et al., 2009, 2012). We divide the continuous data into 30s-time windows and run the beamforming for each time window to get the slowness and azimuth information of the signals. Compared to tremors in subduction zones, the tremor signal in the Central San Andreas fault generally has a shorter duration. Thus, to remove the earthquakes from the tremor detections, we treat the signal as tremor when it shows nearly consistent slowness (+/- 0.02 s/km) and azimuth (+/- 10 degrees) in continuous four-time windows, with a window exception considering the possible interference from other types of signals during the 2.5 minutes.

For locating these events, a vector from the center of the array to the azimuth of the maximum amplitude in the slowness space is projected onto the nearest fault. For an estimate of the SAF, we estimate a 2D vertical fault with a strike trending along N30W, parallel to the creeping section in SAF. We exact a vertically homogeneous velocity model to map the slowness values on the fault plane. The beam back-projection algorithm identifies the location with the minimum misfit function between the slowness values mapped on the fault and the projected slowness from the array (Ghosh, Vidale, Sweet, Creager, Wech, & Houston, 2010).

The beam-back projection (BBP) technique was applied on the frequency domain at this array to detect and locate tremors in high resolution (Ghosh et al., 2009, 2012). We have processed the array data using the BBP method for the first nine months – April to December 2013 and presented here. After converting them to usable Seismic Analysis Code (SAC) format, they were filtered in the range of 4-12 Hz, which was the dominant range of frequency with a high signal-to-noise ratio for the tremor in this area. This frequency range is determined using spectral analysis. We first perform beamforming to determine the slowness vector (Gerstoft & Tanimoto, 2007; Johnson & Dudgeon, 1993) and then back-project the slowness vectors to determine their location (Ghosh et al., 2009, 2012). We use the vertical channel with 30 seconds of non-overlapping sliding time windows. Although we developed an automatic algorithm, we randomly checked many events visually to verify tremors. The verification is a two-step process: first, detected tremor signals are visually verified (Figure 5). Then, the beams (Figure 6) were created for these time windows to check their energy distribution in the slowness space.

4.4 Results

In total, we detected 46.2 hours of tremor activity in 262 days analyzed for 2013. On average, we detected 10.6 mins of tremor daily. During the same time, the ECC method (TremorScope project) detected 10.5 hours of tremor, with a daily average of 2.5 minutes. Hence, our array can detect 4.4 times more duration of tremor activity without using any other surface or borehole stations. This is a conservative estimate. Our algorithm can easily be tweaked to detect more than five times the duration of tremor activity. In this case, the likelihood of false detection will go up. Perhaps more importantly, we have been able to

find possible shallow tremors (Figure 4.2, 4.5) in the seismogenic zone where the earthquakes occur. We have visually verified the shallow tremor and checked their location, including depth, by calibrating them using regular fast cataloged earthquakes. In addition, we found LFEs occurring both at the deep and shallow parts of the fault. They are found visually scanning the data and located using the Hypoinverse algorithm, independent of the beam back-projection method. Both shallow and deep LFEs are located in the general area showing tremor activity.

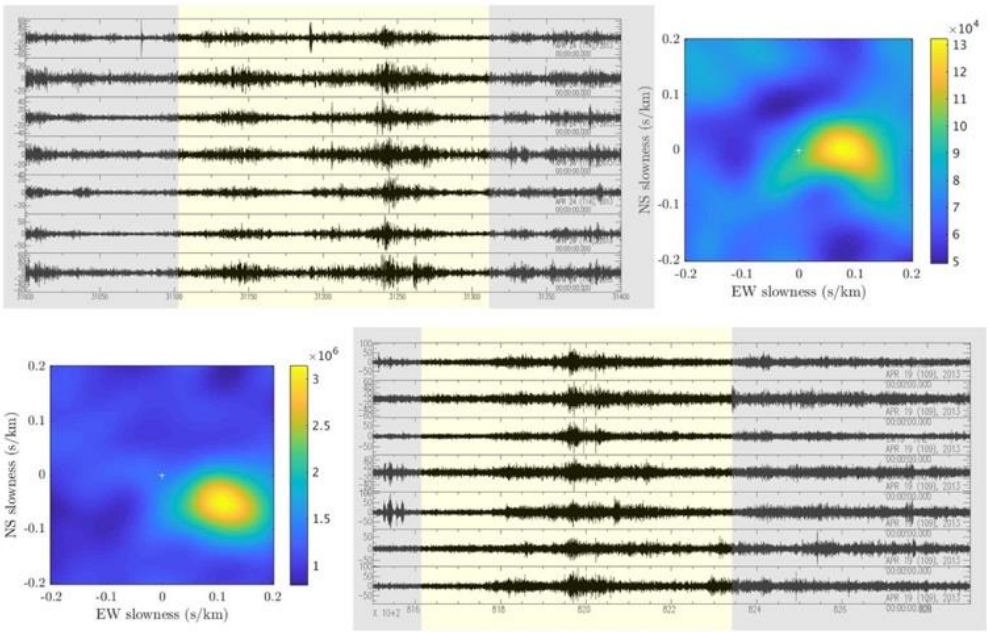

Figure 4.2: This above graph depicts two tremor events- Top Panel: Shallow tremors signal and slowness map showing lower slowness value; Bottom Panel: Deeper tremors signal and slowness map showing higher slowness.

The azimuthal variation of the tremor sources from clustered and uncalibrated results (Figure 4.3) shows that most tremor points in the highly active Cholame region. A

significant number of tremor events occurred northwest of Cholame, indicating array resolving tremor signal northward as far as 100 km from the array. After locating and projecting these tremors on the fault, we were able to identify a group of shallow tremors, and these appear to be consistently repeating in time. A comprehensive analysis of these tremors will revise our understanding of slow earthquake localization in SAF and its frictional behavior.

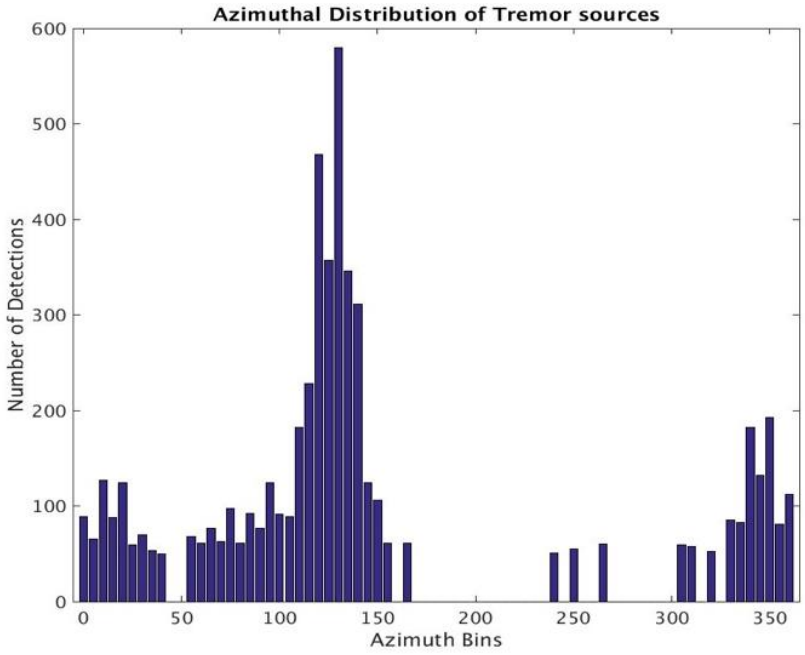

Figure 4.3: The azimuthal distribution of tremors as recorded by the Cholame array and detected using Beam Back Projection

To find LFEs, we first filtered the tremor time windows in the frequency band of 2-8 Hz and then searched for LFE signals visually. We locate the selected events using the first arrivals of body waves (mainly S-waves with a few P-waves). We used one station from the Cholame array and all the surface and borehole stations in the area that recorded the LFE. The selected template events (an example in Figure 4.4) are then used to find

hundreds of more similar events in time using a match filter technique (Shelly et al., 2007a). Matched events are stacked to obtain a cleaner version of the LFE signal for each family (figure 4.4).

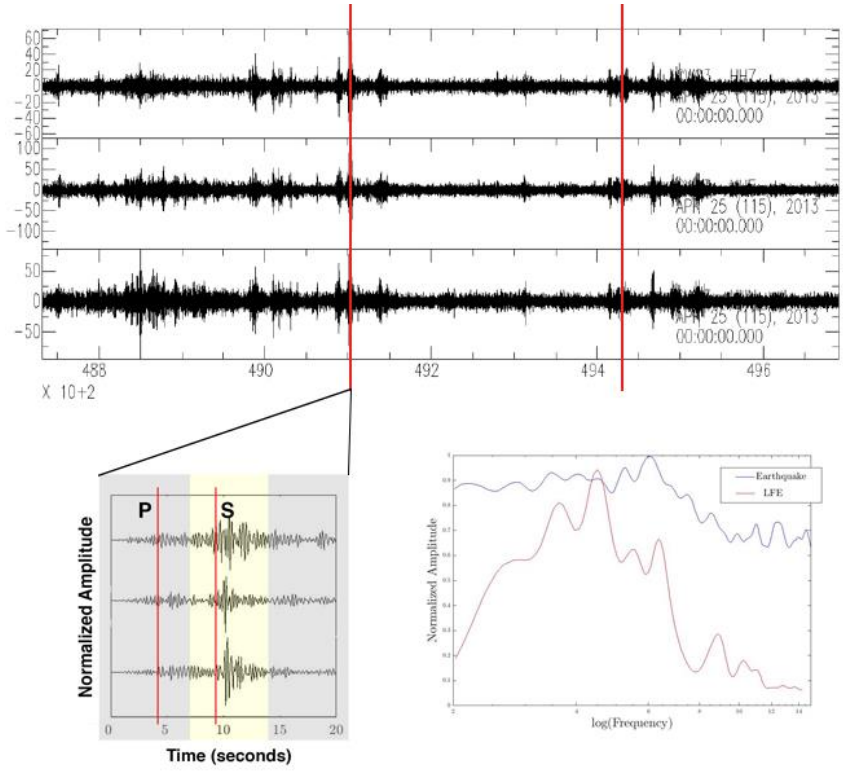

Figure 4.4: Top: A burst of LFE recorded by a station in Cholame. The three panels are the two horizontal channels and one vertical channel. Bottom Left: A stacked LFE signal from the Cholame array, Cholame, CA. Right: The frequency spectrum of the signal showing dominant energy in the 2 to 6 Hz band characteristics of an LFE in comparison in blue which is the energy contained in a local earthquake.

We found three separate shallow and five deep LFE sources not included in the previously published catalog (Shelly, 2017). Locations of the LFEs are shown in Figure 4.5a. We stacked LFE signals for each family to improve the precision of first arrivals

using additional stations to obtain a better absolute location. On top of that, we have used hypoInverse and hypoDD to locate them.

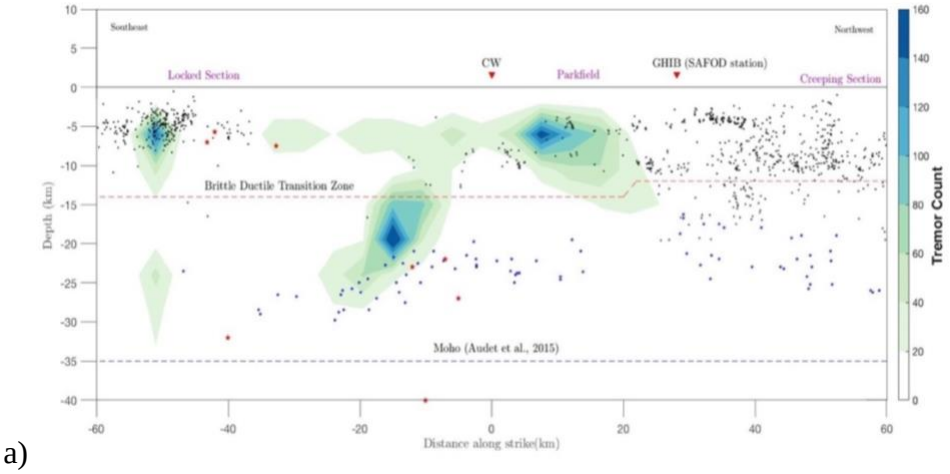

a)

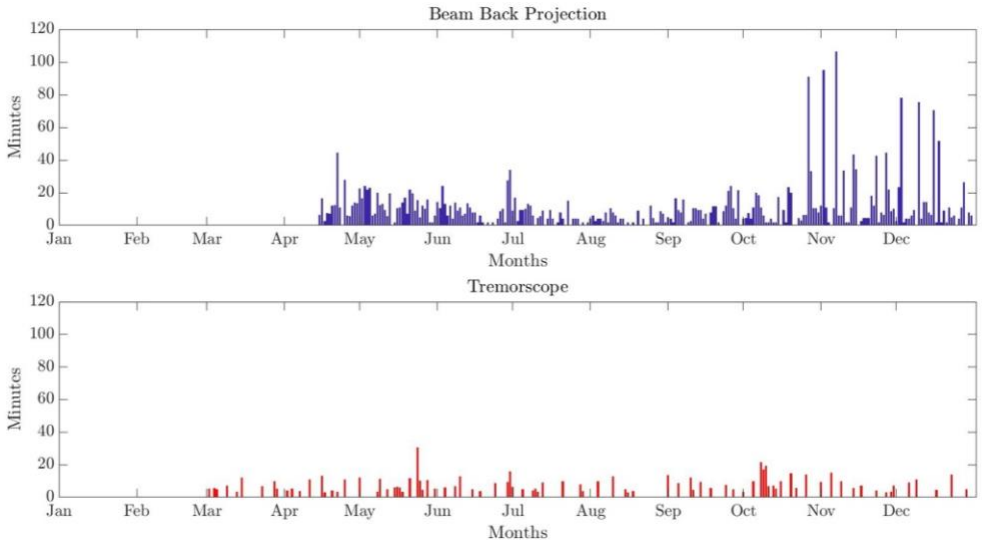

b)

Figure 4.5: a) graph depicts the along strike variation of the tremors on San Andreas Fault. The contour lines depict the tremor patches, and the color indicates the number of tremor episodes. The black stars depict the general seismicity in the area and the RED stars mark the LFE locations. The blue stars mark the LFE's detected by Shelly et al., 2017. b) graph depicts the amount of detection by BBP for a year. Bottom: Graph depicting the minutes of detection of tremors per day using ECC (Tremorscope Catalog).

4.5 Discussion and Conclusion

Envelope cross-correlation (ECC) and match filter methods are used to detect tremors and Low-frequency earthquakes (LFEs) in the Cholame and Parkfield area in central California (Nadeau & Guilhem, 2009; Shelly et al., 2007a, 2009). However, these methods cannot capture the entire level of tremor activity occurring in the area spatially and temporally (Figure 4.5b). Our results show five times more detections than the conventional ECC method. The use of beam back-projection (BBP) has helped us to identify shallow tremors (Figure 4.2,4.5) that have never been observed before in this area. We have strong evidence showing persistent shallow tremor activity in the seismogenic zone with our high-resolution seismic array. This is a rare observation globally (Plata-Martinez et al., 2021; Yamashita et al., 2021) and the first indication of possible direct evidence of bimodal behavior shown by a shallow part of the SAF that repeatedly produces large damaging earthquakes. Understanding how shallow tremor affects the stress dynamics would change our understanding about the interactions of slow and fast earthquakes at SAF. These differing slip behaviors likely reflect different frictional properties within the seismogenic zone. The presence of shallow tremors shows the existence of slowly slipping patches amongst the fast-slipping asperities which was also observed before (Veedu & Barbot, 2016). Triggered tremors due to tidal (Thomas et al., 2009) and teleseismic (Joan Gomberg et al., 2008; Guilhem & Nadeau, 2012; Z. Peng et al., 2008; Zhao et al., 2010) stress perturbations show that the fault is extremely sensitive to small changes, suggesting the presence of high fluid pressure in the fault zone at depths. The presence of fluids are the likely cause of such a variation in frictional locking in

shallow seismogenic sections of the crust. As pointed out earlier, the detectability of the method used for understanding the tremor distribution is crucial in these studies as it may often give rise to artifacts due to low sensitivity to signals. In addition to high sensitivity, the beam back-projection method also scans for tremor activity thoroughly, both spatially and temporally. That is why this method consistently detects approximately five times more tremor activity compared to the visual or ECC method in Cascadia, Alaska, and SAF (Ghosh et al., 2009, 2012; Li & Ghosh, 2017); that is why this method can detect spontaneous tremor under SJF when other methods fail (Hutchison & Ghosh, 2017). In order to obtain a robust catalog a stringent criterion has been applied to avoid coherent noise signal to be detected in this method. Although tremors have a dominant frequency range however they can even vary within the same area. More tremors are likely occurring over the same time period but not detected for various reasons, which includes poor signal-to-noise ratio and limitations of the method used here. Regardless of undetected events, shallow tremors constitute a vital part of the seismic signature of slow earthquakes and present an opportunity to study their source physics. This opens up new avenues to study mechanisms controlling slow earthquakes, frictional properties in the transition zone, and the physics of fault motion in the complex slow and fast slipping central San Andreas Fault.

CHAPTER 5

An automatic Detection code for Very Low Frequency Earthquake using a Centroid Moment Tensor Inversion algorithm (Auto-CMTI)

5.1 Introduction

Very Low frequency earthquakes (VLFEs) are a form of slow earthquakes that often contribute a significant amount of stress release in a tectonic setting. These events have most of their energy in the low frequency band of 0.02 - 0.05 Hz and are challenging to detect and locate using the conventional methods used for fast or regular earthquakes. VLFEs have been occurring in many subduction zones, and these serve as essential stress markers. VLFEs are a part of the slow slip spectra; however, they release a significant amount of moment compared to tremors and low frequency earthquakes. For example, in Cascadia, we see episodic tremors and slip (ETS) continuing for days to weeks and VLFEs with moment equivalent to weeks of tremors; however, despite being an active subduction zone, it has been surprisingly quiet in terms of regular earthquakes. Thus, the VLFEs observed in this region in earlier studies (REF) are crucial to understanding the stress release mechanism in this region. But due to time and computation complexities, the VLFE catalog is not as complete as it may have been, missing out on many events in the vicinity. Thus, to understand how these slow slipping events contribute to the big picture, we needed a better detection capability, which became the motivation of this work.

Centroid Moment tensor inversion is a prevalent method often used while dealing which such events, and it provides a very accurate result. However, there exist several

limitations that restrict the usage of this algorithm. These limitations include the extent of the target area, the number of stations combination, checking the robustness of a detected signal, and final verification to be an actual repeating signal. Furthermore, all these steps have often been done as a separate unit, which is time-consuming and prone to systematic errors. However, in this work, we have developed an automated centroid moment tensor inversion code referred to as aCMT in the rest of the paper. This algorithm compiles all the units mentioned earlier and brings a complete package that can detect VLFEs much more quickly and easily.

Here we use a couple of datasets to verify and detect previously cataloged events. First, we use the time from Hutchison and Ghosh, 2019 to test our code and establish its robustness. And secondly, we use another dataset from Ridgecrest to test for false detection.

5.2 Data

For this analysis, we have used data from broadband stations onshore Cascadia subduction zone and near the July 4tth and 6th Ridgecrest earthquake sequences. These two datasets have been chosen strategically to obtain a positive and a negative detection. The Cascadia subduction zone data is from the 2011 VLFE events as observed by (Ghosh et al., 2015; Hutchison & Ghosh, 2016). We are trying to detect actual events from the data using the Automated CMTI code developed in this project. We are using the 1st 4 VLFE events as a reference to check the validity of our code. The Ridgecrest data serve as a control experiment, and we use the timeline of a couple of weeks starting up to the 4th of

July 2019 earthquake to show the detection capability of this code. As a final check we used a third dataset to detect and locate the recently discovered VLFEs in offshore Cascadia using OBSs.

5.3 Methodology

5.3.1 Centroid Moment Tensor Inversion

Centroid Moment tensor inversion is based on the relationship between six zeroth order basis moment tensor of the earthquake source and the elastic vibrations associated with the earthquakes itself. Hence a seismogram $s_z(t)$ recorded at a station z, can be expressed as convolution of a of the Greens Function of the medium to an impulsive source G with a moment tensor element 'n for source r decomposed into m elements.

$$s_z(t) = \sum_m G^s_{zm}(t) n^r_m \,,$$

Here we divide our target area into 1km by 1km along latitude and longitude, 1km spacing along depth and assume that the source of the vent occurs at one of these grid points. By assuming a pure deviatoric tensor we can arrive at the following equation:

$$m = [G^T G]^{-1} G^T s \,,$$

Here G is the kernel matrix comprising the Greens' function, s is the data vector and m consists of the six independent basis moment tensors.

Using the above equation and comparing the observed waveforms to the synthetic waveform at each grid point we can calculate the variance reduction which can be defined by the following relationship

$$V.R. = \left(1 - \frac{\sum_z \int (s_z(t) - o_z(t))^2 dt}{\sum_z \int (o_z(t))^2 dt}\right) \times 100 \,,$$

Where sz(t) and oz(t) are the original and synthetic seismograms. Then we calculate the moment tensor for each of the grid point using a90 seconds sliding time wine and 1 s time step. The final solution is based on the V.R. and the percentage Compensated Linear vector Dipole (CLVD) which show the degree of similarity and residual radiation from the best double couple source model.

5.3.2 Automated CMTI

In this work, we developed an automated centroid moment tensor inversion code. The input parameters include the target area, list of stations, and the time frame of interest. After the input parameters are established, the code works in three steps; Initial grid search, a reiteration of the results with a more refined grid space to check the consistency of results, and the final step are to match-filter the detected event (Figure 5.1).

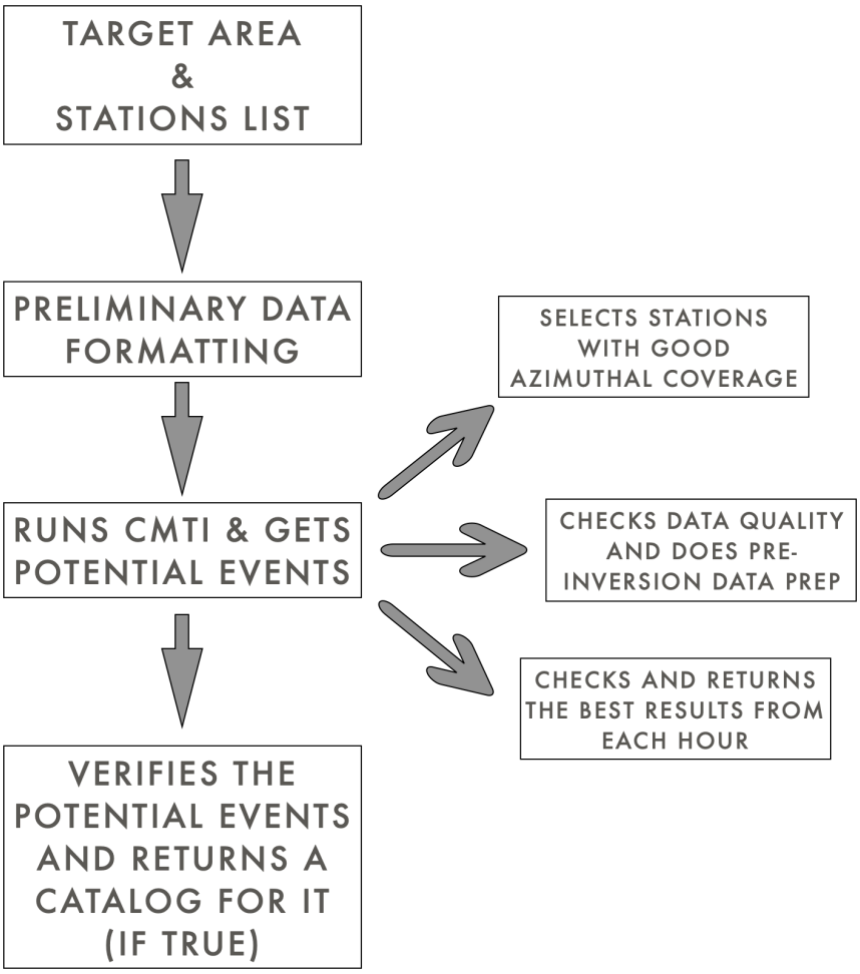

Figure 5.1: The flow chart shows the working of the code in a simplified manner. All these steps show how complicated the process of finding VLFE is, and all these stages have been combined to work in unison in this project.

5.3.3 Initial Grid Search

The first section of the code divides our target area into grid points based on the grid-spacing value given in the input parameters. We start with an initial spacing of 0.1 degrees both in latitude and longitude and broadband stations' list (Figure 5.2). Next, we compute the centroid moment tensor inversion solution for every combination of stations on each grid point.

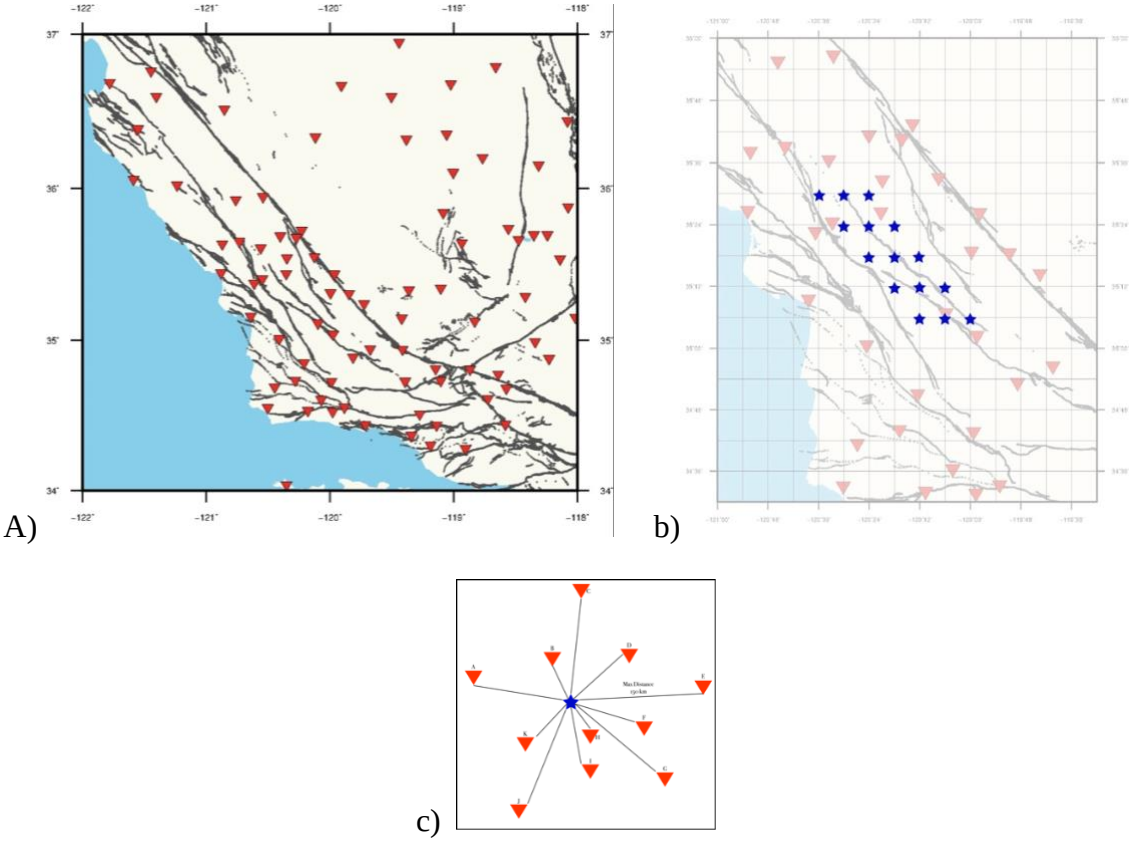

Figure 5.2: a) Show an area of interest to search for VLFEs with stations marked with red triangles. B) Map show the grid points (blue stars) that we are hoping along while doing our search. C) Map show the distribution of all stations around one grid point that is going to be used in a combination of 3-4 stations as per users' choice.

The stations are chosen preferably such that it is in all four quadrants; however, if the station distribution is not good, it will select the next closest station. After the CMTI solution has been computed for every grid point with every possible station combination, the code compiles the best results with a potential event and then prepares for the following code step.

5.3.4 Reiterated Solution of Potential Events

The best potential events are then selected, and their solution is recalculated using a refined grid with the same stations. Finally, the two solutions are compared, and if the events' time, location, and focal mechanism are consistent, the event passes as a valid detection. The potential solutions are selected based on specific values, including variance reduction and CLVD. Thus, all possible events will have a positive VR and CLVD, and their VR will always be greater than CLVD. These same criteria are enforced in the reiteration step to flag out events that might have passed the first stage. Finally, each event is used in match filtering to find repeats in the next step.

5.3.5 Match Filtering

We use each detected VLFE event as a template to perform cross-correlation type matched filtered analysis applying a fast algorithm known as Super-Efficient Cross-correlation (SEC-C; Senobari et al., 2019). Each template event consists of 3 channel broadband data in the best moment tensor inversion solution. Each template is compared to continuous waveform data from the same respective stations and channels as the template event with a sliding time window. Time windows with values above a determined threshold value are cataloged as VLFEs. The threshold for a positive detection using noise templates must be done separately since the background noise would vary from region to region. Once the event passes through all the criteria, a catalog of events is created and reported to the user as a valid detection.

5.4 Results and Discussion

We applied the aCMTI on broadband stations in Cascadia and we were able to detect first 4 VLFEs in the month of August 2011 as reported in Hutchison and Ghosh 2016 (ex. Figure 5.3). These events were passed through all the selection criterion and emerged as positive detections with exact spatial and temporal coordinates as cataloged before. The waveform similarity and focal mechanisms are also exactly similar however the timing and the depth has an error of ~3 units each which is attributed to the difference in the initial processing of raw data.

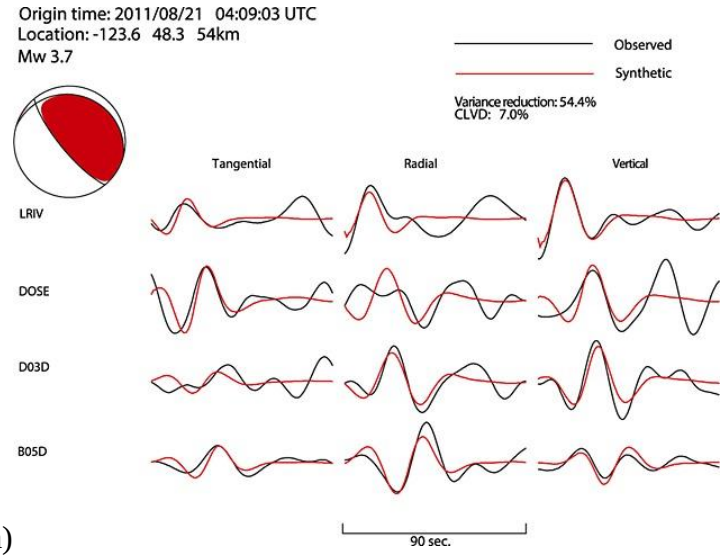

a)

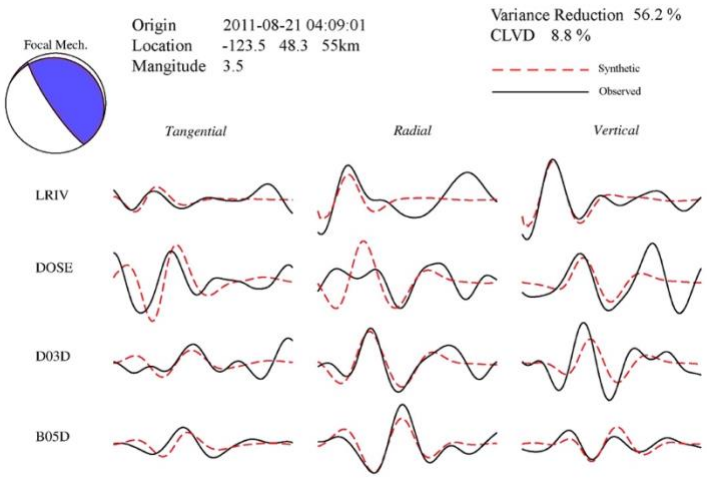

b)

Figure 5.3: a) The panel shows the detection from (Ghosh et al., 2015) (08/21/11T04:09:03). b) This panel shows the automatic detection made by code package created in this work.

Along with the detections it also generates a list of all combinations of stations that have produced the exact event. This algorithm was also tested on the recently discovered VLFEs in Cascadia (in review K. Chaudhuri and Ghosh, 2022) using OBS stations to obtain exact solutions. To test for false negatives, we applied the aCMTI to broadband stations within a 50 km radius of the July 4th Mw 6.4 Ridgecrest earthquake. This area is not known for having any form of slow slip hence will serve as an excellent test to see if the algorithm generates false detections.

5.5 Conclusion

This paper presents an algorithm which can detect and locate VLFE events very precisely with all possible combinations of stations with broadband data. It presents a composite wrapper which excludes the need of running multiple independent algorithms to test the accuracy of the solutions. The accurate detection of cataloged events shows the robustness of this package, and the scope of the search can now extend to various places of the earth. VLFEs are very discrete but important signals which are difficult to detect. Finding more of these events in various tectonic settings are going to be beneficial in the understanding of the frictional behavior of tectonic plates.

CHAPTER 6

6.1 Conclusions

The broad slip spectrum of earthquakes and resulting stress released remain poorly understood. Our understanding about frictional behavior of plates has been modified in the last couple of decades and many new discoveries are improving the state of earthquake science. This dissertation gives a glimpse of the plethora of information that might help ascertain the mechanics of this complex fault behavior. Observations show that a significant part of slow slip was previously not accounted for and further analysis show that they often are spatially and/or temporally related to regular fast earthquakes.

In Cascadia our analysis has revealed the existence of 12 distinct VLFEs along offshore CSZ. We observe a widespread occurrence of offshore VLFEs even in the short timespan analyzed. The VLFEs are mainly clustered offshore and near the trench area. These VLFEs are a vital stress marker considering the lack of regular fast micro-earthquakes in this area. The presence of offshore VLFEs in the CSZ clearly indicates that a significant amount of stress is released by these slowly slipping events that were unknown before this study. CSZ has been tranquil over the past century, with only a few instrumentally recorded micro-earthquakes on the plate interface. However, paleoseismic studies indicate that this margin has hosted ~M_w 9 megathrust earthquakes at 200-500yr intervals with persistent rupture segment boundaries (Adams, 1990; Atwater, 1987; Goldfinger et al., 2012). The Discovery of VLFEs offshore Cascadia opens new avenues to explore mechanisms controlling slow earthquakes, frictional properties along the entire

Cascadia subduction fault including the seismogenic and transition zone, and the physics of fault motion.

In Taiwan slow slip in the form of tremors has been observed to occur around the location of a major earthquake (C. H. Lin, 2012; W. Peng et al., 2019). Ide et al., 2015 use centroid moment tensor inversion on stacked tremor seismograms and identified energy in the VLF spectrum. These tremor windows were proposed to be always concurrent with VLFEs in Taiwan (Ide et al., 2008, 2015). However, with the discovery of discretely identifiable VLFEs, we observe additional interesting connections between slow and fast earthquakes. Our analyses in this study indicate that heightened activity of these deep events leads to the regional shallow earthquake swarms observed in the area. However, temporal relationship between VLFE and tremors activity remain unclear. VLFEs are relatively deep events, and their activity presumably loads the shallower seismogenic crust (Rogers & Dragert, 2003). The Taiwan foreland basin, to the east of the thrust front, is highly active. This activity is often attributed to the presence of yielding over thrusted lower crust on the upper crust (A. T. Lin & Watts, 2002; Yeh et al., 1998). The observed spatio-temporal pattern indicates that the VLFEs at the base of the fault is likely influencing the seismic activity in the seismogenic crust updip. This observation is conclusive of the fact that VLFEs, as a part of the slow spectrum, significantly affects seismogenic crust. Hence more thorough observation with better instrumentation should be done to understand their behavior.

In the Cholame and Parkfield area of central California, ECC and match filter methods have earlier been used to detect tremors and Low-frequency earthquakes (LFEs)

(Nadeau & Guilhem, 2009; Shelly et al., 2007a, 2009). However, these methods cannot capture the entire level of tremor activity occurring in the area spatially and temporally. Our results show five times more detections than the conventional ECC method. The use of beam back-projection (BBP) has helped us to identify shallow tremors that have never been observed before in this area. We have strong evidence showing persistent shallow tremor activity in the seismogenic zone with our high-resolution seismic array. This is a rare observation globally (Plata-Martinez et al., 2021; Yamashita et al., 2021) and the first indication of possible direct evidence of bimodal behavior shown by a shallow part of the SAF that repeatedly produces large damaging earthquakes.

Finally, first 2 projects inspired me to create an automatic VLFE detection code which can detect locate and match filter these events. It presents a composite wrapper which eliminates the need for running multiple independent algorithms to test the accuracy of the solutions. The accurate detection of cataloged events shows the robustness of this package, and the scope of the search can now extend to various places of the earth. The slow earthquake spectrum remains still an open subject and more observations will lead to our detailed understanding of these events.

Bibliography

Adams, J. (1990). Paleoseismicity of the Cascadia Subduction Zone: Evidence from turbidites off the Oregon-Washington Margin. Tectonics, 9(4). https://doi.org/10.1029/TC009i004p00569

Aguiar, A. C., Chao, K., & Beroza, G. C. (2017). Tectonic tremor and LFEs on a reverse fault in Taiwan. Geophysical Research Letters, 44(13). https://doi.org/10.1002/2016GL072148

Ando, M., Tu, Y., Kumagai, H., Yamanaka, Y., & Lin, C. H. (2012). Very low frequency earthquakes along the Ryukyu subduction zone. Geophysical Research Letters, 39(4). https://doi.org/10.1029/2011GL050559

Atwater, B. F. (1987). Evidence for great holocene earthquakes along the outer coast of Washington state. Science, 236(4804). https://doi.org/10.1126/science.236.4804.942

Audet, P., Bostock, M. G., Mercier, J. P., & Cassidy, J. F. (2008). Morphology of the explorer - Juan de Fuca slab edge in northern Cascadia: Imaging plate capture at a ridge-trench-transform riple junction. Geology, 36(11). https://doi.org/10.1130/G25356A.1

Baba, S., Takeo, A., Obara, K., Matsuzawa, T., & Maeda, T. (2020). Comprehensive Detection of Very Low Frequency Earthquakes Off the Hokkaido and Tohoku Pacific Coasts, Northeastern Japan. Journal of Geophysical Research: Solid Earth, 125(1). https://doi.org/10.1029/2019JB017988

Bebout, G. E., & Penniston-Dorland, S. C. (2016). Fluid and mass transfer at subduction interfaces-The field metamorphic record. In Lithos (Vols. 240–243). https://doi.org/10.1016/j.lithos.2015.10.007

Beyssac, O., Simoes, M., Avouac, J. P., Farley, K. A., Chen, Y. G., Chan, Y. C., & Goffé, B. (2007). Late Cenozoic metamorphic evolution and exhumation of Taiwan. Tectonics, 26(6). https://doi.org/10.1029/2006TC002064

Bouchon, M., Karabulut, H., Aktar, M., Özalaybey, S., Schmittbuhl, J., & Bouin, M. P. (2011). Extended nucleation of the 1999 Mw 7.6 Izmit earthquake. Science, 331(6019). https://doi.org/10.1126/science.1197341

Brown, J. R., Beroza, G. C., Ide, S., Ohta, K., Shelly, D. R., Schwartz, S. Y., Rabbel, W., Thorwart, M., & Kao, H. (2009). Deep low-frequency earthquakes in tremor localize to the plate interface in multiple subduction zones. Geophysical Research Letters, 36(19). https://doi.org/10.1029/2009GL040027

Burgette, R. J., Weldon, R. J., & Schmidt, D. A. (2009). Interseismic uplift rates for western Oregon and along-strike variation in locking on the Cascadia subduction zone. Journal of Geophysical Research: Solid Earth, 114(1). https://doi.org/10.1029/2008JB005679

Chao, K., Peng, Z., Wu, C., Tang, C. C., & Lin, C. H. (2012). Remote triggering of non-volcanic tremor around Taiwan. Geophysical Journal International, 188(1). https://doi.org/10.1111/j.1365-246X.2011.05261.x

Chen, W. S., Yeh, J. J., & Syu, S. J. (2019). Late Cenozoic exhumation and erosion of the Taiwan orogenic belt: New insights from petrographic analysis of foreland basin sediments and thermochronological dating on the metamorphic orogenic wedge. Tectonophysics, 750. https://doi.org/10.1016/j.tecto.2018.09.003

Chuang, L. Y., Chen, K. H., Wech, A., Byrne, T., & Peng, W. (2014). Ambient tremors in a collisional orogenic belt. Geophysical Research Letters, 41(5). https://doi.org/10.1002/2014GL059476

Doran, A. K., & Laske, G. (2017). Ocean-bottom seismometer instrument orientations via automated rayleigh-wave arrival-angle measurements. Bulletin of the Seismological Society of America, 107(2). https://doi.org/10.1785/0120160165

Dragert, H., Wang, K., & James, T. S. (2001). A silent slip event on the deeper Cascadia subduction interface. Science, 292(5521). https://doi.org/10.1126/science.1060152

Ekström, G., & Busby, R. W. (2008). Measurements of seismometer orientation at USArray transportable array and backbone stations. Seismological Research Letters, 79(4). https://doi.org/10.1785/gssrl.79.4.554

Fagereng, Å., & Den Hartog, S. A. M. (2017). Subduction megathrust creep governed by pressure solution and frictional-viscous flow. Nature Geoscience, 10(1). https://doi.org/10.1038/ngeo2857

Feng, L., Newman, A. V., Protti, M., Gonzlez, V., Jiang, Y., & Dixon, T. H. (2012). Active deformation near the Nicoya Peninsula, northwestern Costa Rica, between 1996 and 2010: Interseismic megathrust coupling. In Journal of Geophysical Research: Solid Earth (Vol. 117, Issue 6). https://doi.org/10.1029/2012JB009230

Fletcher, J. B., & Baker, L. M. (2010). Analysis of nonvolcanic tremor on the San Andreas fault near Parkfield, CA using U. S. Geological Survey Parkfield Seismic Array. Journal of Geophysical Research: Solid Earth, 115(10). https://doi.org/10.1029/2010JB007511

Frank, W. B. (2016). Slow slip hidden in the noise: The intermittence of tectonic release. Geophysical Research Letters, 43(19). https://doi.org/10.1002/2016GL069537

Gerstoft, P., & Tanimoto, T. (2007). A year of microseisms in southern California. Geophysical Research Letters, 34(20). https://doi.org/10.1029/2007GL031091

Ghosh, A., Huesca-Pérez, E., Brodsky, E., & Ito, Y. (2015). Very low frequency earthquakes in Cascadia migrate with tremor. Geophysical Research Letters, 42(9). https://doi.org/10.1002/2015GL063286

Ghosh, A., Vidale, J. E., & Creager, K. C. (2012). Tremor asperities in the transition zone control evolution of slow earthquakes. Journal of Geophysical Research: Solid Earth, 117(10). https://doi.org/10.1029/2012JB009249

Ghosh, A., Vidale, J. E., Peng, Z., Creager, K. C., & Houston, H. (2009). Complex nonvolcanic tremor near Parkfield, California, triggered by the great 2004 Sumatra earthquake. Journal of Geophysical Research: Solid Earth, 114(12). https://doi.org/10.1029/2008JB006062

Ghosh, A., Vidale, J. E., Sweet, J. R., Creager, K. C., Wech, A. G., & Houston, H. (2010). Tremor bands sweep Cascadia. Geophysical Research Letters, 37(8). https://doi.org/10.1029/2009GL042301

Ghosh, A., Vidale, J. E., Sweet, J. R., Creager, K. C., Wech, A. G., Houston, H., & Brodsky, E. E. (2010). Rapid, continuous streaking of tremor in Cascadia. Geochemistry, Geophysics, Geosystems, 11(12). https://doi.org/10.1029/2010GC003305

Goldfinger, C., Kulm, L. D., Yeats, R. S., McNeill, L., & Hummon, C. (1997). Oblique strike-slip faulting of the central Cascadia submarine forearc. Journal of Geophysical Research: Solid Earth, 102(B4). https://doi.org/10.1029/96jb02655

Goldfinger, C., Nelson, C. H., Morey, A. E., Johnson, J. E., Patton, J. R., Karabanov, E., Gutiérrez-Pastor, J., Eriksson, A. T., Grácia, E., Dunhill, G., Enkin, R. J., Dallimore, A., & Vallier, T. (2012). Turbidite Event History—Methods and Implications for Holocene Paleoseismicity of the Cascadia Subduction Zone: U.S. Geological Survey Professional Paper 1661-F. Earthquake Hazards of the Pacific Northwest Coastal and Marine Regions, 1.

Gomberg, J., Agnew, D. C., & Schwartz, S. Y. (2016). Alternative source models of very low frequency events. Journal of Geophysical Research: Solid Earth, 121(9). https://doi.org/10.1002/2016JB013001

Gomberg, J., Creager, K., Sweet, J., Vidale, J., Ghosh, A., & Hotovec, A. (2012). Earthquake spectra and near-source attenuation in the Cascadia subduction zone. Journal of Geophysical Research: Solid Earth, 117(5). https://doi.org/10.1029/2011JB009055

Gomberg, Joan, Rubinstein, J. L., Peng, Z., Creager, K. C., Vidale, J. E., & Bodin, P. (2008). Widespread triggering of nonvolcanic tremor in California. In Science (Vol. 319, Issue 5860). https://doi.org/10.1126/science.1149164

Guilhem, A., & Nadeau, R. M. (2012). Episodic tremors and deep slow-slip events in Central California. Earth and Planetary Science Letters, 357–358. https://doi.org/10.1016/j.epsl.2012.09.028

Gurevich, B., Makarynska, D., De Paula, O. B., & Pervukhina, M. (2010). A simple model for squirt-flow dispersion and attenuation in fluid-saturated granular rocks. Geophysics, 75(6). https://doi.org/10.1190/1.3509782

Han, S., Bangs, N. L., Carbotte, S. M., Saffer, D. M., & Gibson, J. C. (2017). Links between sediment consolidation and Cascadia megathrust slip behaviour. Nature Geoscience, 10(12), 954–959. https://doi.org/10.1038/s41561-017-0007-2

Han, S., Carbotte, S. M., Canales, J. P., Nedimović, M. R., & Carton, H. (2018). Along-Trench Structural Variations of the Subducting Juan de Fuca Plate From Multichannel

Seismic Reflection Imaging. Journal of Geophysical Research: Solid Earth, 123(4). https://doi.org/10.1002/2017JB015059

Han, S., Carbotte, S. M., Canales, J. P., Nedimovic, M. R., Carton, H., Gibson, J. C., & Horning, G. W. (2016). Seismic reflection imaging of the Juan de Fuca plate from ridge to trench: New constraints on the distribution of faulting and evolution of the crust prior to subduction. Journal of Geophysical Research: Solid Earth, 121(3). https://doi.org/10.1002/2015JB012416

Hayakawa, M., Hattori, K., & Ohta, K. (2007). Monitoring of ULF (ultra-low-frequency) geomagnetic variations associated with earthquakes. Sensors, 7(7). https://doi.org/10.3390/s7071108

Hayman, N. W., & Lavier, L. L. (2014). The geologic record of deep episodic tremor and slip. Geology, 42(3). https://doi.org/10.1130/G34990.1

Hirose, H., Hirahara, K., Kimata, F., Fujii, N., & Miyazaki, S. (1999). A slow thrust slip event following the two 1996 Hyuganada earthquakes beneath the Bungo Channel, southwest Japan. Geophysical Research Letters, 26(21). https://doi.org/10.1029/1999GL010999

Hirose, H., & Obara, K. (2010). Recurrence behavior of short-term slow slip and correlated nonvolcanic tremor episodes in western Shikoku, southwest Japan. Journal of Geophysical Research: Solid Earth, 115(6). https://doi.org/10.1029/2008JB006050

Huesca-Pérez, E., & Ghosh, A. (2015). Crustal anisotropy from tectonic tremor under Washington State in the Cascadia. Geophysical Research Letters, 42(7). https://doi.org/10.1002/2014GL062614

Husen, S., & Kissling, E. (2002). Postseismic fluid flow after the large subduction earthquake of Antofagasta, Chile. Geology, 29(9). https://doi.org/10.1130/0091-7613(2001)029<0847:PFFATL>2.0.CO;2

Hutchison, A. A. (2020). Interepisodic Tremor and Slip Event Episodes of Quasi-spatiotemporally Discrete Tremor and Very Low Frequency Earthquakes in Cascadia Suggestive of a Connective Underlying, Heterogeneous Process. Geophysical Research Letters, 47(3). https://doi.org/10.1029/2019GL086798

Hutchison, A. A., & Ghosh, A. (2016). Very low frequency earthquakes spatiotemporally asynchronous with strong tremor during the 2014 episodic tremor and slip event in Cascadia. Geophysical Research Letters, 43(13). https://doi.org/10.1002/2016GL069750

Hutchison, A. A., & Ghosh, A. (2017). Ambient tectonic tremor in the san jacinto fault, near the anza gap, detected by multiple mini seismic arrays. Bulletin of the Seismological Society of America, 107(5). https://doi.org/10.1785/0120160385

Hutchison, A. A., & Ghosh, A. (2019). Repeating VLFEs During ETS Events in Cascadia Track Slow Slip and Continue Throughout Inter-ETS Period. Journal of Geophysical Research: Solid Earth, 124(1), 554–565. https://doi.org/10.1029/2018JB016138

Ide, S. (2016). Characteristics of slow earthquakes in the very low frequency band: Application to the Cascadia subduction zone. Journal of Geophysical Research: Solid Earth, 121(8), 5942–5952. https://doi.org/10.1002/2016JB013085

Ide, S., Beroza, G. C., Shelly, D. R., & Uchide, T. (2007). A scaling law for slow earthquakes. Nature, 447(7140). https://doi.org/10.1038/nature05780

Ide, S., Imanishi, K., Yoshida, Y., Beroza, G. C., & Shelly, D. R. (2008). Bridging the gap between seismically and geodetically detected slow earthquakes. Geophysical Research Letters, 35(10). https://doi.org/10.1029/2008GL034014

Ide, S., Shelly, D. R., & Beroza, G. C. (2007). Mechanism of deep low frequency earthquakes: Further evidence that deep non-volcanic tremor is generated by shear slip on the plate interface. Geophysical Research Letters, 34(3). https://doi.org/10.1029/2006GL028890

Ide, S., Yabe, S., Tai, H. J., & Chen, K. H. (2015). Thrust-type focal mechanisms of tectonic tremors in Taiwan: Evidence of subduction. Geophysical Research Letters, 42(9). https://doi.org/10.1002/2015GL063794

Ito, Y., Obara, K., Matsuzawa, T., & Maeda, T. (2009). Very low frequency earthquakes related to small asperities on the plate boundary interface at the locked to aseismic transition. Journal of Geophysical Research: Solid Earth, 114(11). https://doi.org/10.1029/2008JB006036

Johnson, D. H. D. H., & Dudgeon, D. E. (1993). Array signal processing: concepts and techniques. In Book.

Kao, H., Wang, K., Dragert, H., Kao, J. Y., & Rogers, G. (2010). Estimating seismic moment magnitude (Mw) of tremor bursts in northern Cascadia: Implications for the "seismic efficiency" of episodic tremor and slip. Geophysical Research Letters, 37(19). https://doi.org/10.1029/2010GL044927

Kato, A., & Nakagawa, S. (2014). Multiple slow-slip events during a foreshock sequence of the 2014 Iquique, Chile Mw 8.1 earthquake. Geophysical Research Letters, 41(15). https://doi.org/10.1002/2014GL061138

Kato, A., Obara, K., Igarashi, T., Tsuruoka, H., Nakagawa, S., & Hirata, N. (2012). Propagation of slow slip leading up to the 2011 Mw 9.0 Tohoku-Oki earthquake. Science, 335(6069). https://doi.org/10.1126/science.1215141

Katsumata, A., & Kamaya, N. (2003). Low-frequency continuous tremor around the Moho discontinuity away from volcanoes in the southwest Japan. Geophysical Research Letters, 30(1). https://doi.org/10.1029/2002gl015981

Kleinrock, M. C., & Hey, R. N. (1989). Detailed tectonics near the tip of the Galapagos 95.5°W propagator: how the lithosphere tears and a spreading axis develops. Journal of Geophysical Research, 94(B10). https://doi.org/10.1029/jb094ib10p13801

Kostoglodov, V., Husker, A., Shapiro, N. M., Payero, J. S., Campillo, M., Cotte, N., & Clayton, R. (2010). The 2006 slow slip event and nonvolcanic tremor in the Mexican subduction zone. Geophysical Research Letters, 37(24). https://doi.org/10.1029/2010GL045424

Kundu, B., Ghosh, A., Mendoza, M., Bürgmann, R., Gahalaut, V. K., & Saikia, D. (2016). Tectonic tremor on Vancouver Island, Cascadia, modulated by the body and surface waves of the Mw 8.6 and 8.2, 2012 East Indian Ocean earthquakes. Geophysical Research Letters, 43(17). https://doi.org/10.1002/2016GL069755

La Rocca, M., Galluzzo, D., Malone, S., McCausland, W., & Del Pezzo, E. (2010). Array analysis and precise source location of deep tremor in Cascadia. Journal of Geophysical Research: Solid Earth, 115(6). https://doi.org/10.1029/2008JB006041

La Rocca, M., Galluzzo, D., Malone, S., McCausland, W., Saccorotti, G., & Del Pezzo, E. (2008). Testing small-aperture array analysis on well-located earthquakes, and application to the location of deep tremor. Bulletin of the Seismological Society of America, 98(2). https://doi.org/10.1785/0120060185

La Rocca, M., McCausland, W., Galluzzo, D., Malone, S., Saccorotti, G., & Del Pezzo, E. (2005). Array measurements of deep tremor signals in the Cascadia subduction zone. Geophysical Research Letters, 32(21). https://doi.org/10.1029/2005GL023974

Li, B., & Ghosh, A. (2017). Near-continuous tremor and low-frequency earthquake activities in the Alaska-Aleutian subduction zone revealed by a mini seismic array. Geophysical Research Letters, 44(11). https://doi.org/10.1002/2016GL072088

Lin, A. T., & Watts, A. B. (2002). Origin of the West Taiwan basin by orogenic loading and flexure of a rifted continental margin. Journal of Geophysical Research: Solid Earth, 107(B9). https://doi.org/10.1029/2001jb000669

Lin, C. H. (2012). The possible observation of slow slip events prior to the occurrence of the 1999 Chi-Chi earthquake. Terrestrial, Atmospheric and Oceanic Sciences, 23(2), 145–159. https://doi.org/10.3319/TAO.2011.09.23.01(T)

Ludwin, R. S. (2004). PNSN, Pacific Northwest Seismograph Network. In Fact Sheet. https://doi.org/10.3133/fs20043073

MacKay, M. E. (1995). Structural variation and landward vergence at the toe of the Oregon accretionary prism. Tectonics, 14(6). https://doi.org/10.1029/95TC02320

MacKay, M. E., Moore, G. F., Cochrane, G. R., Casey Moore, J., & Kulm, L. V. D. (1992). Landward vergence and oblique structural trends in the Oregon margin accretionary prism: Implications and effect on fluid flow. Earth and Planetary Science Letters, 109(3–4). https://doi.org/10.1016/0012-821X(92)90108-8

Matsuzawa, T., Asano, Y., & Obara, K. (2015). Very low frequency earthquakes off the Pacific coast of Tohoku, Japan. Geophysical Research Letters, 42(11). https://doi.org/10.1002/2015GL063959

Maury, J., Ide, S., Cruz-Atienza, V. M., Kostoglodov, V., González-Molina, G., & Pérez-Campos, X. (2016). Comparative study of tectonic tremor locations: Characterization of slow earthquakes in Guerrero, Mexico. Journal of Geophysical Research: Solid Earth, 121(7). https://doi.org/10.1002/2016JB013027

McCaffrey, R., King, R. W., Payne, S. J., & Lancaster, M. (2013). Active tectonics of northwestern U.S. inferred from GPS-derived surface velocities. Journal of Geophysical Research: Solid Earth, 118(2), 709–723. https://doi.org/10.1029/2012JB009473

McCrory, P. A., Blair, J. L., Waldhauser, F., & Oppenheimer, D. H. (2012). Juan de Fuca slab geometry and its relation to Wadati-Benioff zone seismicity. Journal of Geophysical Research: Solid Earth, 117(9). https://doi.org/10.1029/2012JB009407

McGuire, J. J., Collins, J. A., Davis, E., Becker, K., & Heesemann, M. (2018). A Lack of Dynamic Triggering of Slow Slip and Tremor Indicates That the Shallow Cascadia Megathrust Offshore Vancouver Island Is Likely Locked. Geophysical Research Letters, 45(20). https://doi.org/10.1029/2018GL079519

Mendoza, M. M., Ghosh, A., & Rai, S. S. (2016). Dynamic triggering of small local earthquakes in the central Himalaya. Geophysical Research Letters, 43(18). https://doi.org/10.1002/2016GL069969

Michel, S., Gualandi, A., & Avouac, J. P. (2019). Interseismic Coupling and Slow Slip Events on the Cascadia Megathrust. Pure and Applied Geophysics, 176(9). https://doi.org/10.1007/s00024-018-1991-x

Nadeau, R. M., & Dolenc, D. (2005). Nonvolcanic tremors deep beneath the San Andreas Fault. Science, 307(5708). https://doi.org/10.1126/science.1107142

Nadeau, R. M., & Guilhem, A. (2009). Nonvolcanic tremor evolution and the San Simeon and Parkfield, California, earthquakes. Science, 325(5937). https://doi.org/10.1126/science.1174155

Nakajima, J., Yoshida, K., & Hasegawa, A. (2013). An intraslab seismic sequence activated by the 2011 Tohoku-oki earthquake: Evidence for fluid-related embrittlement. Journal of Geophysical Research: Solid Earth, 118(7). https://doi.org/10.1002/jgrb.50246

Nakano, M., Hori, T., Araki, E., Kodaira, S., & Ide, S. (2018). Shallow very-low-frequency earthquakes accompany slow slip events in the Nankai subduction zone /704/2151/210 /704/2151/508 article. Nature Communications, 9(1). https://doi.org/10.1038/s41467-018-03431-5

Nedimović, M. R., Bohnenstiehl, D. W. R., Carbotte, S. M., Pablo Canales, J., & Dziak, R. P. (2009). Faulting and hydration of the Juan de Fuca plate system. Earth and Planetary Science Letters, 284(1–2), 94–102. https://doi.org/10.1016/j.epsl.2009.04.013

Nippress, S. E. J., & Rietbrock, A. (2007). Seismogenic zone high permeability in the Central Andes inferred from relocations of micro-earthquakes. Earth and Planetary Science Letters, 263(3–4). https://doi.org/10.1016/j.epsl.2007.08.032

Nishikawa, T., Matsuzawa, T., Ohta, K., Uchida, N., Nishimura, T., & Ide, S. (2019). The slow earthquake spectrum in the Japan Trench illuminated by the S-net seafloor observatories. Science, 365(6455). https://doi.org/10.1126/science.aax5618

Nuyen, C. P., & Schmidt, D. A. (2021). Filling the Gap in Cascadia: The Emergence of Low-Amplitude Long-Term Slow Slip. Geochemistry, Geophysics, Geosystems, 22(3). https://doi.org/10.1029/2020GC009477

Obara, K. (2002). Nonvolcanic deep tremor associated with subduction in southwest Japan. Science, 296(5573). https://doi.org/10.1126/science.1070378

Ozawa, S., Murakami, M., & Tada, T. (2001). Time-dependent inversion study of the slow thrust event in the Nankai trough subduction zone, southwestern Japan. Journal of Geophysical Research: Solid Earth, 106(B1). https://doi.org/10.1029/2000jb900317

Payero, J. S., Kostoglodov, V., Shapiro, N., Mikumo, T., Iglesias, A., Pérez-Campos, X., & Clayton, R. W. (2008). Nonvolcanic tremor observed in the Mexican subduction zone. Geophysical Research Letters, 35(7). https://doi.org/10.1029/2007GL032877

Peng, W., Chen, K. H., & Toda, S. (2019). Evaluating the Association Between Tectonic Tremors and Earthquakes in Taiwan From 7 Years Catalogs. Journal of Geophysical Research: Solid Earth, 124(4). https://doi.org/10.1029/2018JB017258

Peng, Z., & Gomberg, J. (2010). An integrated perspective of the continuum between earthquakes and slow-slip phenomena. In Nature Geoscience (Vol. 3, Issue 9). https://doi.org/10.1038/ngeo940

Peng, Z., Vidale, J. E., Creager, K. C., Rubinstein, J. L., Gomberg, J., & Bodin, P. (2008). Strong tremor near Parkfield, CA, excited by the 2002 Denali Fault earthquake. Geophysical Research Letters, 35(23). https://doi.org/10.1029/2008GL036080

Peterson, C. L., McNutt, S. R., & Christensen, D. H. (2011). Nonvolcanic tremor in the Aleutian arc. Bulletin of the Seismological Society of America, 101(6). https://doi.org/10.1785/0120100241

Plata-Martinez, R., Ide, S., Shinohara, M., Garcia, E. S., Mizuno, N., Dominguez, L. A., Taira, T., Yamashita, Y., Toh, A., Yamada, T., Real, J., Husker, A., Cruz-Atienza, V. M., & Ito, Y. (2021). Shallow slow earthquakes to decipher future catastrophic earthquakes in the Guerrero seismic gap. Nature Communications, 12(1). https://doi.org/10.1038/s41467-021-24210-9

Plourde, A. P., Bostock, M. G., Audet, P., & Thomas, A. M. (2015). Low-frequency earthquakes at the southern Cascadia margin. Geophysical Research Letters, 42(12). https://doi.org/10.1002/2015GL064363

Ringler, A. T., Hutt, C. R., Persefield, K., & Gee, L. S. (2013). Seismic station installation orientation errors at ANSS and IRIS/USGS stations. Seismological Research Letters, 84(6). https://doi.org/10.1785/0220130072

Rivet, D., Campillo, M., Shapiro, N. M., Cruz-Atienza, V., Radiguet, M., Cotte, N., & Kostoglodov, V. (2011). Seismic evidence of nonlinear crustal deformation during a large slow slip event in Mexico. Geophysical Research Letters, 38(8). https://doi.org/10.1029/2011GL047151

Rogers, G., & Dragert, H. (2003). Episodic tremor and slip on the Cascadia subduction zone: The chatter of silent slip. Science, 300(5627). https://doi.org/10.1126/science.1084783

Rubinstein, J. L., Shelly, D. R., & Ellsworth, W. L. (2009). Non-volcanic Tremor: A Window into the Roots of Fault Zones. In New Frontiers in Integrated Solid Earth Sciences. https://doi.org/10.1007/978-90-481-2737-5_8

Ruiz, S., Metois, M., Fuenzalida, A., Ruiz, J., Leyton, F., Grandin, R., Vigny, C., Madariaga, R., & Campos, J. (2014). Intense foreshocks and a slow slip event preceded the 2014 Iquique Mw8.1 earthquake. Science, 6201. https://doi.org/10.1126/science.1256074

Schmalzle, G. M., McCaffrey, R., & Creager, K. C. (2014). Central Cascadia subduction zone creep. Geochemistry, Geophysics, Geosystems, 15(4). https://doi.org/10.1002/2013GC005172

Schwartz, S. Y., & Rokosky, J. M. (2007). Slow slip events and seismic tremor at circum-pacific subduction zones. In Reviews of Geophysics (Vol. 45, Issue 3). https://doi.org/10.1029/2006RG000208

Senobari, N. S., Funning, G. J., Keogh, E., Zhu, Y., Yeh, C. C. M., Zimmerman, Z., & Mueen, A. (2019). Super-efficient cross-correlation (SEC-C): A fast matched filtering code suitable for desktop computers. Seismological Research Letters, 90(1). https://doi.org/10.1785/0220180122

Shapiro, S. A., Huenges, E., & Borm, G. (1997). Estimating the crust permeability from fluid-injection-induced seismic emission at the KTB site. Geophysical Journal International, 131(2). https://doi.org/10.1111/j.1365-246X.1997.tb01215.x

Shelly, D. R. (2017). A 15 year catalog of more than 1 million low-frequency earthquakes: Tracking tremor and slip along the deep San Andreas Fault. Journal of Geophysical Research: Solid Earth, 122(5). https://doi.org/10.1002/2017JB014047

Shelly, D. R., Beroza, G. C., & Ide, S. (2007a). Complex evolution of transient slip derived from precise tremor locations in western Shikoku, Japan. Geochemistry, Geophysics, Geosystems, 8(10). https://doi.org/10.1029/2007GC001640

Shelly, D. R., Beroza, G. C., & Ide, S. (2007b). Non-volcanic tremor and low-frequency earthquake swarms. Nature, 446(7133). https://doi.org/10.1038/nature05666

Shelly, D. R., Beroza, G. C., Ide, S., & Nakamula, S. (2006). Low-frequency earthquakes in Shikoku, Japan, and their relationship to episodic tremor and slip. Nature, 442(7099). https://doi.org/10.1038/nature04931

Shelly, D. R., Ellsworth, W. L., Ryberg, T., Haberland, C., Fuis, G. S., Murphy, J., Nadeau, R. M., & Bürgmann, R. (2009). Precise location of San Andreas Fault tremors near Cholame, California using seismometer clusters: Slip on the deep extension of the fault? Geophysical Research Letters, 36(1). https://doi.org/10.1029/2008GL036367

Sibson, R. H. (2013). Stress switching in subduction forearcs: Implications for overpressure containment and strength cycling on megathrusts. Tectonophysics, 600. https://doi.org/10.1016/j.tecto.2013.02.035

Sieh, K. E. (1978). Slip Along the San Andreas Fault Associated with the Great 1857 Earthquake. Bulletin of the Seismological Society of America, 68(5).

Stone, I., Vidale, J. E., Han, S., & Roland, E. (2018). Catalog of Offshore Seismicity in Cascadia: Insights Into the Regional Distribution of Microseismicity and its Relation to Subduction Processes. Journal of Geophysical Research: Solid Earth, 123(1). https://doi.org/10.1002/2017JB014966

Sweet, J. R., Creager, K. C., & Houston, H. (2014). A family of repeating low-frequency earthquakes at the downdip edge of tremor and slip. Geochemistry, Geophysics, Geosystems, 15(9). https://doi.org/10.1002/2014GC005449

Takeo, A., Idehara, K., Iritani, R., Tonegawa, T., Nagaoka, Y., Nishida, K., Kawakatsu, H., Tanaka, S., Miyakawa, K., Iidaka, T., Obayashi, M., Tsuruoka, H., Shiomi, K., & Obara, K. (2010). Very broadband analysis of a swarm of very low frequency earthquakes and tremors beneath Kii Peninsula, SW Japan. Geophysical Research Letters, 37(6). https://doi.org/10.1029/2010GL042586

Tang, C. C., Peng, Z., Chao, K., Chen, C. H., & Lin, C. H. (2010). Detecting low-frequency earthquakes within non-volcanic tremor in southern Taiwan triggered by the 2005 Mw8.6 Nias earthquake. Geophysical Research Letters, 37(16). https://doi.org/10.1029/2010GL043918

Tape, C., Holtkamp, S., Silwal, V., Hawthorne, J., Kaneko, Y., Ampuero, J. P., Ji, C., Ruppert, N., Smith, K., & West, M. E. (2018). Earthquake nucleation and fault slip complexity in the lower crust of central Alaska. Nature Geoscience, 11(7). https://doi.org/10.1038/s41561-018-0144-2

Thomas, A. M., Nadeau, R. M., & Bürgmann, R. (2009). Tremor-tide correlations and near-lithostatic pore pressure on the deep San Andreas fault. Nature, 462(7276). https://doi.org/10.1038/nature08654

Veedu, D. M., & Barbot, S. (2016). The Parkfield tremors reveal slow and fast ruptures on the same asperity. Nature, 532(7599). https://doi.org/10.1038/nature17190

Walter, J. I., Schwartz, S. Y., Protti, M., & Gonzalez, V. (2013). The synchronous occurrence of shallow tremor and very low frequency earthquakes offshore of the Nicoya Peninsula, Costa Rica. Geophysical Research Letters, 40(8). https://doi.org/10.1002/grl.50213

Warner, M. (2004). Free water and seismic reflectivity in the lower continental crust. Journal of Geophysics and Engineering, 1(1). https://doi.org/10.1088/1742-2132/1/1/012

Watt, J. T., & Brothers, D. S. (2020). Systematic characterization of morphotectonic variability along the Cascadia convergent margin: Implications for shallow megathrust behavior and tsunami hazards. Geosphere, 17, 1–23. https://doi.org/10.1130/GES02178.1

Wech, A. G. (2010). Interactive tremor monitoring. Seismological Research Letters, 81(4). https://doi.org/10.1785/gssrl.81.4.664

Wilson, D. S. (1986). A kinematic model for the Gorda Deformation Zone as a diffuse southern boundary of the Juan de Fuca Plate. Journal of Geophysical Research, 91(B10). https://doi.org/10.1029/jb091ib10p10259

Yamamoto, E., Matsumura, S., & Ohkubo, T. (2005). A slow slip event in the Tokai area detected by tilt and seismic observation and its possible recurrence. Earth, Planets and Space, 57(10). https://doi.org/10.1186/BF03351871

Yamashita, Y., Shinohara, M., & Yamada, T. (2021). Shallow tectonic tremor activities in Hyuga-nada, Nankai subduction zone, based on long-term broadband ocean bottom seismic observations. In Earth, Planets and Space (Vol. 73, Issue 1). https://doi.org/10.1186/s40623-021-01533-x

Yeh, Y. H., Shih, R. C., Lin, C. H., Liu, C. C., Yen, H. Y., Huang, B. S., Liu, C. S., Chen, P. Z., Huang, C. S., Wu, C. J., & Wu, F. T. (1998). Onshore/Offshore Wide-Angle Deep

Seismic Profiling in Taiwan. Terrestrial, Atmospheric and Oceanic Sciences, 9(3). https://doi.org/10.3319/TAO.1998.9.3.301(TAICRUST)

Zhao, P., Peng, Z., & Sabra, K. G. (2010). Detecting remotely triggered temporal changes around the Parkfield section of the San Andreas fault. Earthquake Science, 23(5). https://doi.org/10.1007/s11589-010-0748-0